國立臺灣大學電機資訊學院電信工程學研究所

碩士論文

Graduate Institute of Communication Engineering

College of Electrical Engineering and Computer Science

National Taiwan University

Master Thesis

濾波器組多載波系統之濾波器設計使用半正定放寬以壓抑側瓣之峰值

FBMC System Filter Design Minimizing Peak Side-lobe Level using Semidefinite Relaxation

邱善晨

Shan-Chen Chiu

指導教授: 蘇柏青 博士

Advisor: Borching Su, Ph.D.

中華民國 112 年 7 月

July, 2023

doi:10.6342/NTU202302942

國立臺灣大學碩士學位論文
口試委員會審定書
MASTER'S THESIS ACCEPTANCE CERTIFICATE
NATIONAL TAIWAN UNIVERSITY

濾波器多載波系統之濾波器設計使用半正定放寬以壓抑側瓣之峰值

FBMC System Filter Design Minimizing Peak Side-lobe Level using Semidefinite Relaxation

本論文係 邱善晨 (R10942133) 在國立臺灣大學電信工程學研究所完成之碩士學位論文，於民國 112 年 7 月 31 日承下列考試委員審查通過及口試及格，特此證明。

The undersigned, appointed by the Graduate Institute of Communication Engineering on 31th July 2023 have examined a Master's thesis entitled above presented by Shan-Chen Chiu (R10942133) candidate and hereby certify that it is worthy of acceptance.

口試委員 Oral examination committee:

蘇柏青	馮世邁	林源倍
（指導教授 Advisor）		

系主任/所長 Director: 劉深淵

誌謝

在這碩士兩年的歷程中，獲得最多的其實並不是多麼大量的專業知識或技能，而是遇到了許多形形色色的人，他們帶給我正面積極的風度和思維，抑或帶來負面的情緒和散漫的處事態度，這些人都成為了我這兩年下來的學習對象和借鏡，也因為他們帶給我的寶貴經歷，才得以完成這篇論文，謝謝各位。

在碩一時期，我初來乍到，對於不管實驗室的事物，又或者是理論和實驗上的知識都還不足，謝謝林承鈺學長、董庭瑋學姊、陳曦鈞學長、羅政捷學長、黃勁維學長的鼓勵和知識上的分享，時常跟這些學長姊吃飯聊天，都讓我獲得很多收穫和陪伴，也謝謝學長姊於畢業之後也不忘關心還在學的我，讓我能夠繼續堅持進行自己的研究，也謝謝同屆的同學丁文淵時常分享他在於研究上的知識。

在碩二時期，必須要進行自己的論文研究，謝謝指導教授蘇柏青老師帶給我很多研究方面的建議，也於碩士論文的指導上點出很多能改進的地方，讓我能夠以不同的角度和觀點切入自己的研究。

最後，我想要謝謝自己的家人，於我最壓抑的時期能夠給予我諒解和支持，使我能夠重拾勇氣與信念以面對壓力和痛苦，謝謝你們，你們是我最敬愛的親人也是恩人，希望我往後進入職場，能夠回報這份恩情。

doi:10.6342/NTU202302942

doi:10.6342/NTU202302942

摘要

在許多 5G 或者 6G 的會議中，有限的頻寬資源常常是被探討的主題之一，在設計新的通訊系統過程中，我們總是需要將有效的使用頻寬資源的方法考慮進來，而較低的側瓣峰值等級/能量，也就是較低的頻帶外能量，是一個達到高頻譜效率的關鍵點。濾波器多載波系統的傳輸技術已被研究多年，且它在頻譜效能的表現上，要比現在主導寬頻多載波通訊系統領域多年的正交分頻多工系統還要來的好，也許濾波器多載波系統在未來有望能取代正交分頻多工的地位。

濾波器多載波系統的濾波器設計也已經被研究了幾年了，但在設計的過程中仍然有一些非必要的限制存在，如頻譜衰減。在我們的研究中，我們提出了一個嶄新設計濾波器的方式以匹配濾波器多載波系統/偏移正交振福調變系統，它有效的壓低側瓣峰值，也仍保留了近完美解調的性質。我們最後會在模擬結果中呈現在幅度響應和位元錯誤率測試上的表現。

關鍵字：濾波器多載波系統、偏移正交振幅調變、濾波器設計、凸函數最佳化、半正定放寬、側瓣峰值等級、最大側瓣等級

doi:10.6342/NTU202302942

doi:10.6342/NTU202302942

Abstract

Limited spectrum resources are usually the one of main topics covered in 5G or 6G conferences. The process of designing the novel communication system to fit the new regulation should be always concerned with the efficient usage of spectrum resources. Lower peak side-lobe level/power, i.e., lower out-of-band emission (OoBE), is the key point to achieving spectrum efficiency. The filter bank multicarrier (FBMC) transmission technique has been investigated for years, and the spectrum performance of FBMC outperforms the performance of orthogonal frequency division multiplexing (OFDM), a dominant transmission technique for broadband multicarrier communications in recent years. Perhaps FBMC could replace OFDM as a new communication system in the future.

The filter design of FBMC has been researched for years, but there are still some drawbacks in the designing process such as constraints about spectrum decay. In our work, we propose a new method of designing the filter for the FBMC/OQAM system, which efficiently suppresses the peak side-lobe level, but still considers the property of

doi:10.6342/NTU202302942

near-perfect reconstruction. We would show the performance of the magnitude response and bit error rate (BER) test in our simulation result.

Keywords: FBMC(filter bank multicarrier), OQAM(offset QAM), Filter Design, convex optimization, SDR(semidefinite relaxation), PSL(peak side-lobe level), MSL(maximum side-lobe level)

doi:10.6342/NTU202302942

Contents

doi:10.6342/NTU202302942

doi:10.6342/NTU202302942

doi:10.6342/NTU202302942

doi:10.6342/NTU202302942

List of Figures

doi:10.6342/NTU202302942

doi:10.6342/NTU202302942

List of Tables

doi:10.6342/NTU202302942

doi:10.6342/NTU202302942

Chapter 1 Introduction

doi:10.6342/NTU202302942

1.1 Introduction

Orthogonal Frequency division multiplexing (OFDM) is widely adopted because of a number of advantages that it offers, such as simply eliminating inter-symbol interference (ISI) through the use of a cyclic prefix, computational efficiency by using FFT techniques to implement the modulation and demodulation functions, etc. [7] However, in certain applications such as cognitive radios and uplink of multiuser multicarrier systems, where a subset of subcarriers is allocated to each user OFDM may be an undesirable solution [8]. OFDM is a poor fit because the filters associated with its synthesized subcarrier signals and analyzed subcarrier signals have relatively large side lobes, which will result in out-of-band emission (OoBE) among the bands of different users. The above problems could be greatly alleviated if the filters in the synthesis filter bank and analysis filter bank have small sidelobes. This kind of system with diversely well-designed filters is called filter bank multicarrier (FBMC), whose waveform is regarded as a strong candidate for 5G/6G and other wireless systems to come. FBMC generates lower OoBE by using a non-rectangular pulse and deals with ISI without relying on CP, which makes it more efficient than OFDM.

The filter/waveform design associated with FBMC has been researched for years. Compared with the rectangular filter used by OFDM, the length of filters used by FBMC is usually long. The reason why FBMC uses a long filter can be regarded as improving the behavior of magnitude response by more variables that we can control in the time domain, i.e., FBMC uses more variables to suppress OoBE which is one of the drawbacks of OFDM. In the past decades, there have been many research works on FBMC waveform design [14, 17, 24, 26] that have some good properties. In the early research such as [24],

doi:10.6342/NTU202302942

the authors mathematically investigated the discrete time series of prolate filter thoroughly and designed the filter by concern with maximizing in-band energy in order to suppress the OoBE. In the later work [26], based on [24], the authors aimed to minimize the OoBE but also consider the property of near-perfect reconstruction (NPR) which wasn't considered by previous works. In [17], the authors proposed a well-designed closed-form FBMC prototype filter corresponding to different values of overlapping factor K, and this filter was thoroughly investigated in [1]. Based on the design technique which is a simple intuitive frequency sampling (FS) method, this filter is popular and still the major choice of FBMC waveforms. In the recent work [14], the authors used convex optimization to design the FBMC waveform, which also aimed to minimize OoBE and maintain NPR. Furthermore, they take spectrum decay into account. With this concern, the spectrum decays faster in the region of the stopband. We will show the details of them in Chapter 3.

Even though the FBMC waveform has been researched thoroughly in the past, some aspects could still be improved. In particular, in order to minimize the OoBE interference caused to an adjacent, narrowband user, it would be a good idea to minimize the peak side-lobes (PSLs) of the magnitude response of the prototype filter within the out-of-band regions, rather than minimizing just the total. However, all the previously reported works mentioned in the previous paragraph have not explicitly considered the PSLs as the objective function in an optimization problem. This leads to a possibility that a better prototype filter in terms of an even smaller PSL may exist. For this reason, we propose to minimize all the PSLs in our optimization problem, which is the major aspect we want to improve. In addition, the concern about spectrum decay of magnitude response of the waveform is redundant, which would result in a relatively high maximum side-lobe level (MSL).

doi:10.6342/NTU202302942

That would cause interference to the neighbor communication system or different users. By the way, the SIR of the prototype filters mentioned in the previous paragraph is great enough to achieve NPR that we don't need to enhance the SIR to be too high, which can be observed in the numerical results in Chapter 5.

In this thesis, we propose a novel FBMC waveform design method that achieves a smaller peak side lobe than all existing waveform designs in the literature. The purpose is to minimize the peak side-lobe level (PSL) but also retain the property of near-perfect reconstruction (NPR) for FBMC. We propose to use the semi-definite relaxation (SDR) [19] to solve the primal problem by applying Dattorro Iterative Algorithm [4]. The rest of the thesis is organized as follows. In Chapter 2, the FBMC-OQAM system model is introduced. In Chapter 3, previous works on designing prototype filters for FBMC-OQAM systems are first reviewed, followed by the formulation of the proposed optimization problem of the prototype filter that would meet the aforementioned requirements. In Chapter 4, we introduce the proposed approach to solving the primal problem. In Chapter 5, numerical simulations are conducted to give a fair comparison between the proposed prototype filter and other popular choices mentioned in Chapter 3. Finally, Chapter 6 gives the concluding remarks.

1.2 Notations

Matrices are denoted by upper case bold letters, and column vectors are denoted by lower case bold letters. Superscripts $(\cdot)^*$, $(\cdot)^{-1}$, $(\cdot)^T$ and $(\cdot)^H$ denote conjugate, inverse, transpose, and transpose-conjugate, respectively. Operators $|\cdot|$ and $*$ denote absolute value and 2D convolution respectively. Operators $\uparrow M$ and $\downarrow M$ denote the M-fold

doi:10.6342/NTU202302942

expander and the M-fold decimator, respectively. Operator $\langle a[n]|b[n]\rangle = \sum_{n=-\infty}^{\infty} a[n]b[n]$ denote the inner product of $a[n]$ and $b[n]$. Operators $\lceil\cdot\rceil$ and $\lfloor\cdot\rfloor$ denote ceiling function and floor function respectively. Operators $\Re\{\cdot\}$ and $\Im\{\cdot\}$ denote the real part operation and the imaginary part operation respectively. The function $X(z)$ denotes the z transform of $x[n]$, i.e., $X(z) = \sum_{n=-\infty}^{\infty} x[n]z^{-n}$. We write $x \sim \mathcal{CN}(0, \sigma_n^2)$ to mean that x is a complex Gaussian variable with zero mean and variance σ_n^2. We use $E\{\cdot\}$ to denote the expectation value.

doi:10.6342/NTU202302942

Chapter 2 System Model

doi:10.6342/NTU202302942

In this chapter, we describe the FBMC system model. In Section 2.1, we briefly describe the FBMC transceiver and specify the input/output relation by a block diagram. In Section 2.2, we describe the FBMC system transmitter which contains OQAM modulation and FBMC synthesis filter bank (SFB). In Section 2.3, we describe the FBMC system receiver which contains FBMC analysis filter bank (AFB), subcarrier-wise equalizer, and OQAM demodulation. The main references of the FBMC system model described here include [7, 11]. The prototype filter design problem in the next chapter will be based on the system model described in this chapter. The performance evaluation in terms of BER will also be based on this chapter.

2.1 FBMC System Model

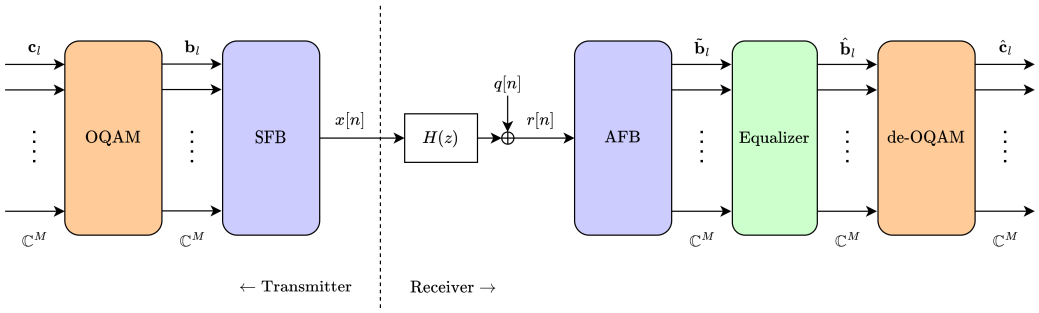

Figure 2.1: Block diagram of FBMC-OQAM transceiver

Figure 2.1 shows the block diagram of an M-subcarrier FBMC-OQAM transceiver. At the transmitter, we denote $\mathbf{c}_l = [c_{0,l}\ c_{1,l}\ \cdots\ c_{M-1,l}]^T \in \mathbb{C}^M$ as the complex QAM symbol vector followed with OQAM processing. We denote $c_{m,l}$ as the complex QAM symbol, where m is the subcarrier index, and l is the time index at the symbol rate. We denote $\mathbf{b}_l = [b_{0,l}\ b_{1,l}\ \cdots\ b_{M-1,l}]^T \in \mathbb{C}^M$ is as the complex OQAM symbol vector. We use $x[n]$ to denote the time domain transmitted signal generated by the sum of the output signal from each subchannel of SFB. At the receiver, the received signal $r[n]$ is obtained

doi:10.6342/NTU202302942

by the sum of additive white Gaussian noise (AWGN) $q[n] \sim \mathcal{CN}(0, \sigma_n^2)$ and the transmitted signal $x[n]$ passing through the linear time-invariant (LTI) channel $H(z)$. After the AFB, we denote $\tilde{\mathbf{b}}_l = [\tilde{b}_{0,l}\ \tilde{b}_{1,l}\ \cdots\ \tilde{b}_{M-1,l}]^T$ as the unestimated OQAM symbol vector. Estimated OQAM symbol vector $\hat{\mathbf{b}}_l = [\hat{b}_{0,l}\ \hat{b}_{1,l}\ \cdots\ \hat{b}_{M-1,l}]^T$ would be obtained by applying equalizer on $\tilde{\mathbf{b}}_l$. Finally, estimated QAM symbol vector $\hat{\mathbf{c}}_l = [\hat{c}_{0,l}\ \hat{c}_{1,l}\ \cdots\ \hat{c}_{M-1,l}]^T$ could be obtained by OQAM demodulation processing.

2.2 FBMC-OQAM Transmitter

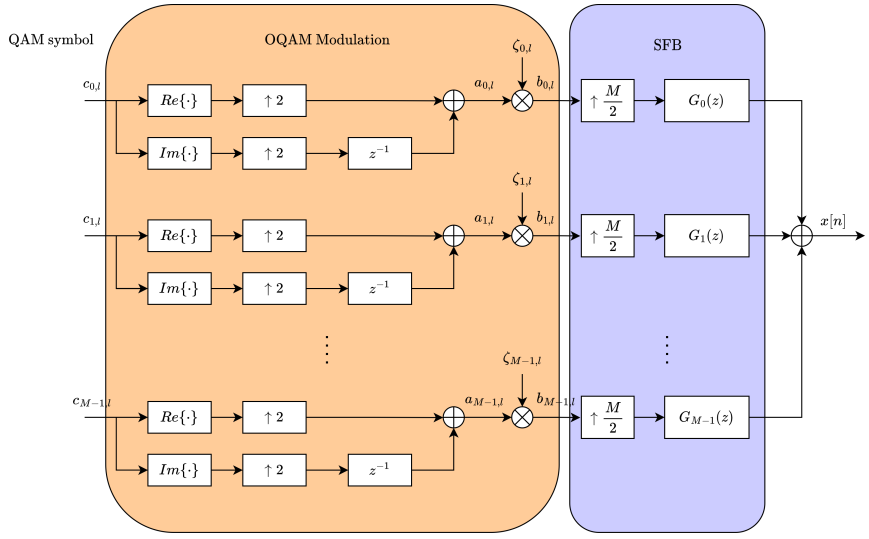

Figure 2.2: Block diagram of FBMC-OQAM transmitter

2.2.1 OQAM Modulation

Figure 2.2 shows the detail of the FBMC-OQAM transmitter. We denote M as the number of FBMC subcarriers and assume that M is chosen as an even integer. At the OQAM processing, QAM symbols $\{c_{m,l}\}_{m=0,\ldots,M-1}$ are divided into the real part and the imaginary part for each subchannel, which could be regarded as two staggered pulse

doi:10.6342/NTU202302942

amplitude modulation (PAM) symbols $\{a_{m,l}\}_{m=0,...,M-1}$. We can express $a_{m,l}$ as

$$\begin{cases} a_{m,2l} = \Re\{c_{m,l}\} \\ a_{m,2l+1} = \Im\{c_{m,l}\}. \end{cases} \tag{2.1}$$

Here, the phase shift term $\{\zeta_{m,l}\}_{m=0,...,M-1}$ is introduced to minimize the interference between adjacent channel. The phase shift term $\zeta_{m,l}$ is written as

$$\zeta_{m,l} = e^{j(m+l)\frac{\pi}{2}} = \begin{cases} \pm 1, & \text{when } (m+l) \text{ is even} \\ \pm j, & \text{when } (m+l) \text{ is odd,} \end{cases} \tag{2.2}$$

which makes sure that the neighboring subcarrier transmits the staggered part (real/imaginary part) of the QAM symbol. This is why the system is also called staggered multitone (SMT) [9]. Finally, the output of OQAM modulation is expressed as

$$b_{m,l} = a_{m,l}\zeta_{m,l}, \quad m = 0, ..., M-1. \tag{2.3}$$

2.2.2 Synthesis Filter Bank (SFB)

The filters designed for FBMC are usually longer than the rectangular filter used by OFDM. Here, we introduce the overlapping factor K used to extend the length of the filter, where K is an integer number greater than one. We can regard the extended filter as more variables to modulate the magnitude response of the filter.

In the stage of SFB, we modulate the OQAM symbols by the upsampler with factor $\frac{M}{2}$ and the transmitting filters $\{G_m(z)\}_{m=0,...,M-1}$. The impulse response of the m-th transmitting filter $G_m(z)$ is expressed as

$$g_m[n] = g[n]e^{j2\pi\frac{m}{M}n}, \quad n = 0, 1, ..., KM-1, \tag{2.4}$$

doi:10.6342/NTU202302942

where $g[n]$ denote real-valued prototype filter coefficients. Then, the transmitted signal is generated by the sum of the signal from each subchannel, and the direct form in the time domain can be expressed as

$$\begin{aligned} x[n] &= \sum_{m=0}^{M-1} \{[a_{m,l}\zeta_{m,l}]_{\uparrow \frac{M}{2}} * g_m[l]\} \\ &= \sum_{m=0}^{M-1} \sum_{l=-\infty}^{\infty} \{[a_{m,l}\zeta_{m,l}]_{\uparrow \frac{M}{2}} g_m[n-l]\} \\ &= \sum_{m=0}^{M-1} \sum_{l=-\infty}^{\infty} a_{m,l}\zeta_{m,l} g[n - l \cdot \frac{M}{2}] e^{j2\pi \frac{m}{M}(n - l \cdot \frac{M}{2})}. \end{aligned} \tag{2.5}$$

2.3 FBMC-OQAM Receiver

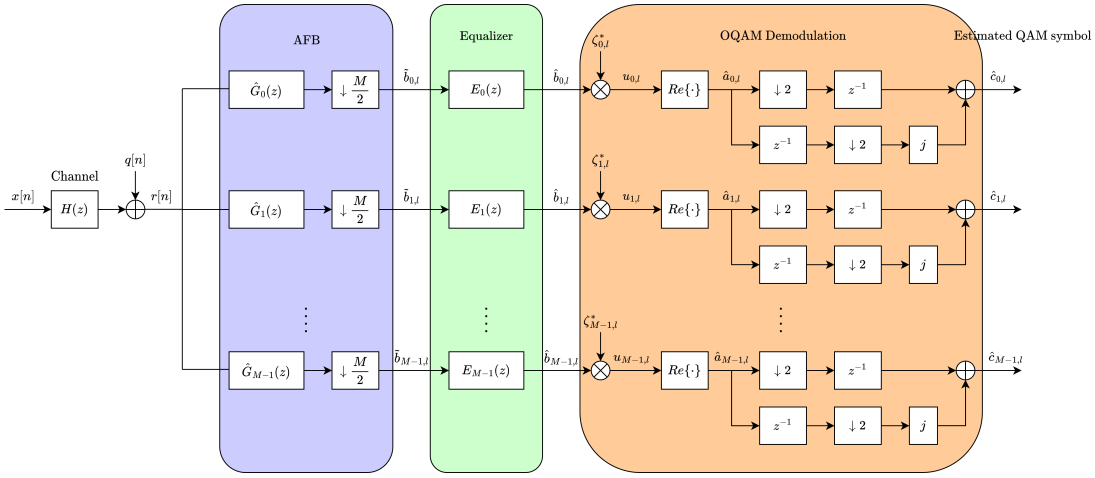

Figure 2.3: Block diagram of FBMC-OQAM receiver

2.3.1 Analysis Filter Bank (AFB)

Figure 2.3 shows the detail of FBMC-OQAM receiver with the LTI channel $H(z)$. At the receiver, received signal $r[n]$ passes through the stage of AFB which consists of receiving filters $\{\hat{G}_m(z)\}_{m=0,1,\ldots,M-1}$ and downsampler with factor $\frac{M}{2}$. The impulse re-

doi:10.6342/NTU202302942

sponse of m-th receiving filter $\hat{G}_m(z)$ is expressed as

$$\hat{g}_m[n] = g_m^*[-n] = g[-n]e^{-j2\pi\frac{m}{M}(-n)}, \quad n = -KM+1, \cdots, -1, 0. \tag{2.6}$$

Then, the m-th unestimated OQAM symbol $\tilde{b}_{m,l}$ can be expressed as

$$\tilde{b}_{m,l} = \sum_{n=-\infty}^{\infty} r[n]\hat{g}_m[l \cdot \frac{M}{2} - n]. \tag{2.7}$$

2.3.2 Equalizer

In this section, we will introduce the equalizer used in the FBMC-OQAM system. We adopt the finite impulse response (FIR) per-subchannel equalizers derived based on the frequency sampling (FS) approach, which was originally introduced in [12], and thoroughly analyzed in [10]. The extended application for the MIMO FBMC-OQAM system can be discovered in [11].

In practice, the communication system would suffer from the distortion caused by the channel effect we want to eliminate. We now analyze the effect in the z-domain for the FBMC-OQAM system. The unestimated OQAM symbol of m-th subchannel in the z-domain can be expressed as

$$\begin{aligned} \tilde{B}_m(z) &= \left[G_m(z)H(z)\hat{G}_m(z)\right]_{\downarrow\frac{M}{2}} B_m(z) \\ &= H_m(z)\left[G_m(z)\hat{G}_m(z)\right]_{\downarrow\frac{M}{2}} B_m(z), \end{aligned} \tag{2.8}$$

doi:10.6342/NTU202302942

where we define the channel effect of m-th subchannel as

$$H_m(z) = \frac{\left[G_m(z)H(z)\hat{G}_m(z)\right]_{\downarrow\frac{M}{2}}}{\left[G_m(z)\hat{G}_m(z)\right]_{\downarrow\frac{M}{2}}}. \tag{2.9}$$

Throughout this thesis, we adopt the zero-forcing (ZF) scheme for the equalizer. The ideal transfer function of the m-th subchannel equalizer is written as

$$E_m(z) = \frac{1}{H_m(z)}. \tag{2.10}$$

Since we cannot take infinite points on the frequency domain to balance the channel effect, we now define the finite target frequency points as

$$\mathbf{\Omega}_{L_w} = \begin{bmatrix}\Omega_0 & \Omega_1 & \cdots & \Omega_{L_w-1}\end{bmatrix}^T = \frac{2\pi}{L_w+1}\mathbf{i}, \quad \mathbf{i} = [1, 2, ..., L_w]^T \tag{2.11}$$

in order to approach the ideal transfer function (2.10), and the FIR transfer function of an L_w-tap equalizer in subchannel m can be expressed as

$$E_m(z) = w_{m,0} + w_{m,1}z^{-1} + \cdots + w_{m,(L_w-1)}z^{-(L_w-1)}, \tag{2.12}$$

where $w_{m,n}$ denote the weight for each tap. Based on (2.12), the weights can be reformulated as a vector form which can be expressed as

$$\mathbf{w}_m = \mathbf{A}^{-1}\mathbf{e}_m, \tag{2.13}$$

where

$$\mathbf{w}_m = [w_{m,0}\ w_{m,1}\ \cdots\ w_{m,L_w-1}]^T \in \mathbb{C}^{L_w}, \tag{2.14}$$

doi:10.6342/NTU202302942

$$\mathbf{A} = \begin{bmatrix} \mathbf{a}_0^T \\ \vdots \\ \mathbf{a}_{L_w-1}^T \end{bmatrix} \in \mathbb{C}^{L_w \times L_w}, \quad \text{with} \quad \mathbf{a}_l^T = \begin{bmatrix} 1 & e^{-j\Omega_l} & \cdots & e^{-j\Omega_l(L_w-1)} \end{bmatrix} \tag{2.15}$$

$$\text{and} \quad \mathbf{e}_m = [E_m(e^{j\Omega_0}) \ \cdots \ E_m(e^{j\Omega_{L_w-1}})]^T. \tag{2.16}$$

Finally, the estimated OQAM symbol in m-th subchannel is written as

$$\hat{b}_{m,l} = \sum_{n=0}^{L_w-1} w_{m,n} \tilde{b}_{m,l-n}. \tag{2.17}$$

2.3.3 OQAM Demodulation

At the OQAM demodulation, the estimated OQAM symbols $\{\hat{b}_{m,l}\}_{m=0,\ldots,M-1}$ are multiplied by the conjugate phase shift term $\{\zeta_{m,l}^*\}_{m=0,\ldots,M-1}$ in each subchannel. Then, the real part operator and the operation of real to complex (R2C) demapping recovered them to become the estimated QAM symbols $\{\hat{c}_{m,l}\}_{m=0,\ldots,M-1}$.

2.3.4 Near perfect reconstruction (NPR)

In all the communication systems, when we conduct them in the case of a perfect channel condition (i.e., when $H(z) = 1$ and $q[n] = 0$), the perfect reconstruction (PR) is the necessary property. If the PR is achieved, the the estimated staggered PAM symbol in m-th subchannel can be written as

$$\hat{a}_{m,l} = a_{m,l} \tag{2.18}$$

doi:10.6342/NTU202302942

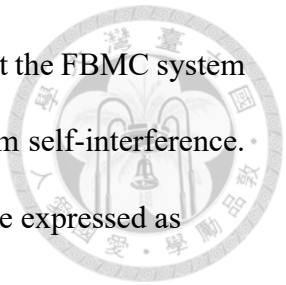

However, due to the extended prototype filter, even though we conduct the FBMC system in the case of a perfect channel condition, the system still suffers from self-interference. Then, the estimated staggered PAM symbol in m-th subchannel can be expressed as

$$\hat{a}_{m,l} = a_{m,l} + \rho_{m,l} \tag{2.19}$$

for all $l \in \mathbb{Z}$, and $\rho_{m,l}$ is denoted as the self-interference term in m-th subchannel. But if we select the well-designed prototype filter $g[n]$ [1, 14, 26], the self-interference term $\rho_{m,l}$ would be small enough to be negligible.

doi:10.6342/NTU202302942

Chapter 3 Previous Works & Problem Formulation

doi:10.6342/NTU202302942

In this chapter, we briefly describe the previous works and problem formulation for our work. In Section 3.1, we introduce several works of FBMC filter design in past decades. Throughout these works, we can find out some constraints that could be modified. In Section 3.2, we propose a novel optimization problem to minimize all the PSL but also achieve NPR that is mentioned in Section 2.3.4. The primal problem formulated in this chapter will be reformulated to be an equivalent form in the next chapter, and we would solve it by the proposed algorithm.

3.1 Previous Works

In this section, we briefly introduce some prototype filter options for the FBMC-OQAM system. We don't provide a full survey on these filters but to realize the method they proposed.

3.1.1 Prolate Filter and Discrete Slepian Sequences

The Prolate filter [24] is a classic design that aims to maximize the energy within the region of the passband. The optimization problem of this design can be expressed as

$$\begin{aligned} \boldsymbol{\psi}_{0,\omega_s} = \text{argmax} \quad & \mathbf{g}^T \boldsymbol{\Gamma}(\omega_s) \mathbf{g} \\ \text{subject to} \quad & \mathbf{g}^T \mathbf{g} = 1, \end{aligned} \tag{3.1}$$

where the definition of $\mathbf{g}$ and $\boldsymbol{\Gamma}(\omega_s)$ can be found in (4.1) and (5.5), respectively. Since $\boldsymbol{\Gamma}(\omega_s)$ is symmetric, a straightforward solution comes by recalling the Rayleigh-Ritz theorem, which guarantees the solution of (3.1) to be the eigenvector associated with the largest eigenvalues of $\boldsymbol{\Gamma}(\omega_s)$. By denoting $\gamma_0 \geq \gamma_1 \geq \cdots \geq \gamma_{KM-1} \geq 0$ as the eigenvalues of

doi:10.6342/NTU202302942

$\mathbf{\Gamma}(\omega_s)$, and $\boldsymbol{\psi}_{i,\omega_s}$ as the eigenvector associated to γ_i, the solution of (3.1) is

$$\boldsymbol{\psi}_{0,\omega_s} = [\psi_{0,\omega_s}[0]\ \psi_{0,\omega_s}[1]\ \cdots\ \psi_{0,\omega_s}[KM-1]]^T, \tag{3.2}$$

and γ_i also represents the normalized energy of $\psi_i[n]$. Indeed, the vector set $\{\boldsymbol{\psi}_{i,\omega_s}[n]\}_i$ is also known as the discrete Prolate spheroidal sequences (DPSS) or the Slepian series.

3.1.2 Optimal Finite Duration Pulse (OFDP)

As stated previously, the Prolate design is optimal in terms of minimizing the energy outside the passband. However, near-perfect reconstruction (NPR) requirements are not taken into account in this design. From this perspective, the OFDP deploys the Slepian series to provide a filter design with low OoB emission and a good symbol reconstruction capability. The OFDP can be written as

$$g[n] = \sum_i \alpha_{2i}\psi_{2i,\omega_s}[n], \tag{3.3}$$

where the coefficients α_{2i} can be found in [25, tab. I].

3.1.3 PHYDYAS/Mirabbasi-Martin filter

To ensure fast spectrum decay at the region of stopband, the Mirabbasi-Martin prototype filter [17] focuses on minimizing the discontinuity in their boundaries while maintaining good reconstruction features for multicarrier applications and ensuring a smooth pulse variation. This design uses the frequency sampling (FS) technique, where the filter weights are actually samples of the frequency response of the prototype filter. The

doi:10.6342/NTU202302942

Mirabbasi-Martin prototype filter can be written as the following discrete low-pass filter

$$g[n] = \begin{cases} k_0 + 2\sum_{i=1}^{K-1} k_i \cos(\frac{2\pi i}{KM} n), & 0 \le n \le L_p - 1 \\ 0, & \text{otherwise} \end{cases}, \tag{3.4}$$

where L_p is the filter length, and the coefficients $\{k_i\}_{i=0,\dots,K-1}$ can be found in [1, 2]. The normalized factor is $k_{nrml} = \sqrt{KM(1 + 2\sum_{i=1}^{K-1} k_i^2)}$ in order to make sure that the power of $g[n]$ to be unity. By the way, when the overlapping factor $K = 4$, in many works [21, 27], authors refer to this filter as the PHYDYAS filter.

3.1.4 Kobayashi's works - via convex optimization

More recently, based on the research of R. T. Kobayashi and T. Abrão [14], a prototype filter design methodology based on convex optimization was proposed. Through this design, they aim to minimize the OoB energy emission, while providing a high-quality symbol reconstruction and maintaining a fast spectrum decay. In order to model the prototype filter, they define the matrix

$$\mathbf{F} = [\mathbf{f}_0 \ \mathbf{f}_1 \ \cdots \ \mathbf{f}_{N-1}] \tag{3.5}$$

to be an aggregation of N sequences, where

$$\mathbf{f}_i = [f_i[0] \ f_i[1] \ \cdots \ f_i[L_p - 1]]^T, \tag{3.6}$$

and they denote $L_p = KM + 1$ as filter length, while the filter length of ours is $L = KM$. Hence, they express the prototype as the linear transformation

$$\mathbf{g} = \mathbf{F}\mathbf{c}, \tag{3.7}$$

doi:10.6342/NTU202302942

where

$$\mathbf{c} = [c_0 \ c_1 \ \cdots \ c_{N-1}]^T \tag{3.8}$$

are the coefficients to be optimized.

Throughout their work, they consider two families to be deployed as $f_i[n]$. First, they consider $f_i[n]$ as the DPSS, i.e.,

$$f_i[n] = \psi_{2i,\omega_s}[n]. \tag{3.9}$$

As an alternative, a family of cosine sequences can also be deployed:

$$f_i[n] = \begin{cases} \frac{1}{\sqrt{KM+1}}, & i = 0 \\ \sqrt{\frac{2}{KM+2}} \cos(\frac{2\pi i}{KM} n), & i = 1, \cdots, N-1. \end{cases} \tag{3.10}$$

Then, their primal problem of designing filter can be expressed as

$$\mathbf{c}^* = \text{argmin} \quad \mathbf{c}^T \mathbf{Q}_0 \mathbf{c} \tag{3.11a}$$

$$\text{subject to} \quad \mathbf{c}^T \mathbf{Q}_{m,n}^{(3a)} \mathbf{c} < \epsilon_0 + \delta, \qquad (m,n) \in \mathcal{E} \tag{3.11b}$$

$$\mathbf{c}^T \mathbf{Q}_{m,n}^{(3b)} \mathbf{c} < \epsilon_0 + \delta, \qquad (m,n) \in \mathcal{E} \tag{3.11c}$$

$$|\mathbf{u}_k^T \mathbf{c}| \leq u_0, \qquad k \in \mathcal{K} \tag{3.11d}$$

$$\mathbf{c}^T \mathbf{F}^T \mathbf{F} \mathbf{c} = 1. \tag{3.11e}$$

The objective function (3.11a) represents the suppression of energy out of the pass-band. The constraints (3.11b) and (3.11c) represent the suppression of the self-interference caused by the extended filter itself. The constraint (3.11d) represents the spectrum decay. The constraint (3.11e) represents the power constraint of the filter. The detail of the variables $\mathbf{Q}_0$, $\mathbf{Q}_{m,n}^{(3a)}$, $\mathbf{Q}_{m,n}^{(3b)}$, ϵ_0, δ, $\mathcal{E}$, $\mathcal{K}$, $\mathbf{u}_k$ and u_0 can be founded in [14]. In this thesis, we

doi:10.6342/NTU202302942

compare the Type-II filter and the Type-III filter from this work with the proposed prototype filter. The optimal coefficients $\{c_i\}_{i=0,\ldots,N-1}$ can be found in [14, tab. IV].

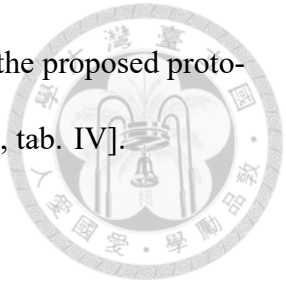

3.2 Problem Formulation

Based on the design techniques introduced in Section 3.1, we could find some aspects worth improving. The major aspect we want to improve is suppressing all the PSLs rather than suppressing the total OoBE. The spectrum decay mentioned in previous work is a redundant constraint, and the main problem is to minimize the interference to the adjacent band.

In this section, we propose a novel prototype filter design method based on convex optimization. The main purpose is to reduce all the PSLs but also provide a high-quality symbol reconstruction. In order to design a better prototype filter, we need to specify the properties of the prototype filter $g[n]$ that it must satisfy. Then, the estimated PAM symbol $\hat{a}_{m,l}\big|_{m=m_0,l=l_0}$ can be expressed as

$$\begin{aligned}
\hat{a}_{m_0,l_0} &= \Re\left\{\left\{\left[r[l] * \hat{g}_{m_0}[l]\right]_{\downarrow\frac{M}{2}}\right\}\Big|_{l=l_0} \cdot \zeta^*_{m_0,l_0}\right\} \\
&= \Re\left\{\left\{\left[\sum_{n=-\infty}^{\infty} r[n]\hat{g}_{m_0}[l-n]\right]_{\downarrow\frac{M}{2}}\right\}\Big|_{l=l_0} \cdot \zeta^*_{m_0,l_0}\right\} \\
&= \Re\left\{\sum_{n=-\infty}^{\infty} r[n]\hat{g}_{m_0}[l_0 \cdot \tfrac{M}{2} - n] \cdot \zeta^*_{m_0,l_0}\right\}.
\end{aligned} \tag{3.12}$$

We first consider the case that the channel is non-distorted and one-tap (non-frequency

doi:10.6342/NTU202302942

selective) without additive noise, i.e., $r[n] = x[n]$. Then, (3.12) can be expressed as

$$\begin{aligned}
&\Re\left\{\sum_{n=-\infty}^{\infty} x[n]\hat{g}_{m_0}[l_0\cdot\tfrac{M}{2}-n]\cdot\zeta^*_{m_0,l_0}\right\}\\
&=\Re\left\{\sum_{n=-\infty}^{\infty}\left\{\sum_{m=0}^{M-1}\sum_{l=-\infty}^{\infty} a_{m,l}\zeta_{m,l}g[n-l\cdot\tfrac{M}{2}]e^{j2\pi\frac{m}{M}(n-l\cdot\frac{M}{2})}\right\}\right.\\
&\quad\left.\cdot g[n-l_0\cdot\tfrac{M}{2}]e^{-j2\pi\frac{m_0}{M}(n-l_0\cdot\frac{M}{2})}\cdot\zeta^*_{m_0,l_0}\right\}\\
&=\Re\left\{\sum_{l=-\infty}^{\infty}\sum_{m=0}^{M-1} a_{m,l}\zeta_{m,l}\zeta^*_{m_0,l_0}e^{-j\pi ml}e^{j\pi m_0 l_0}\right.\\
&\quad\left.\cdot\left(\sum_{n=-\infty}^{\infty} g[n-l\cdot\tfrac{M}{2}]g[n-l_0\cdot\tfrac{M}{2}]e^{j2\pi\frac{(m-m_0)}{M}n}\right)\right\}.
\end{aligned}\tag{3.13}$$

We now replace n by $n+\frac{lM}{2}$, and (3.13) can be expressed as

$$\begin{aligned}
&\Re\left\{\sum_{l=-\infty}^{\infty}\sum_{m=0}^{M-1} a_{m,l}\zeta_{m,l}\zeta^*_{m_0,l_0}e^{-j\pi ml}e^{j\pi m_0 l_0}\right.\\
&\quad\left.\cdot\left(\sum_{n=-\infty}^{\infty} g[n]g[n+(l-l_0)\cdot\tfrac{M}{2}]e^{j2\pi\frac{(m-m_0)}{M}(n+\frac{lM}{2})}\right)\right\}.
\end{aligned}\tag{3.14}$$

By replacing m by $m+m_0$ and l by $l+l_0$, we can rewrite (3.14) as

$$\begin{aligned}
&\Re\left\{\sum_{l=-\infty}^{\infty}\sum_{m=-m_0}^{M-m_0-1} a_{m+m_0,l+l_0}\zeta_{m+m_0,l+l_0}\zeta^*_{m_0,l_0}e^{-j\pi(m+m_0)(l+l_0)}e^{j\pi m_0 l_0}\right.\\
&\quad\left.\cdot\left(\sum_{n=-\infty}^{\infty} g[n]g[n+l\cdot\tfrac{M}{2}]e^{j2\pi\frac{m}{M}(n+\frac{(l+l_0)M}{2})}\right)\right\}\\
&=\Re\left\{\sum_{l=-\infty}^{\infty}\sum_{m=-m_0}^{M-m_0-1} a_{m+m_0,l+l_0}\zeta_{m+m_0,l+l_0}\zeta^*_{m_0,l_0}e^{-j\pi m_0 l}\right.\\
&\quad\left.\cdot\left(\sum_{n=0}^{KM-1} g[n]g[n+l\cdot\tfrac{M}{2}]e^{j2\pi\frac{m}{M}n}\right)\right\}.
\end{aligned}\tag{3.15}$$

From (3.15), we can obtain the estimated staggered PAM symbol $\hat{a}_{m_0,l_0}$ by applying the (Property 1) that the prototype filter must satisfy, and the symbol $\hat{a}_{m_0,l_0}$ can be expressed

doi:10.6342/NTU202302942

as

$$\hat{a}_{m_0,l_0} = a_{m_0,l_0} + \underbrace{\sum_{\substack{l=-\infty \\ |l|+|m|\neq 0}}^{\infty} \sum_{m=-m_0}^{M-m_0-1} a_{m+m_0,l+l_0}(-1)^{m_0 l}}_{\cdot \Re\left\{\zeta_{m+m_0,l+l_0}\zeta^*_{m_0,l_0} \sum_{n=0}^{KM-1} g[n]g[n+l\cdot\frac{M}{2}]e^{j2\pi\frac{m}{M}n}\right\}}, \tag{3.16}$$

ρ_{m_0,l_0} : self-interference

where we denote ρ_{m_0,l_0} as self-interference term for a_{m_0,l_0}. The necessary property used above can be expressed as

$$\sum_{n=0}^{KM-1} g[n]g[n] = 1, \qquad \text{(Property 1)}$$

and we can also regard (Property 1) as a power constraint.

After taking the real part operation, the staggered PAM symbol is expressed as

$$\hat{a}_{m_0,l_0} = a_{m_0,l_0} + \rho_{m_0,l_0}. \tag{3.17}$$

Unfortunately, the undesired self-interference term ρ_{m_0,l_0} is not zero so we cannot eliminate it thoroughly. Therefore, we want to suppress the interference as much as possible to approach the property of near-perfect reconstruction (NPR), which is mentioned in Section 2.3.4. Here, we introduce the discrete ambiguity function in order to simplify the expression of self-interference from (3.16), and it is written as

$$A_{m,l} = \sum_{n=0}^{KM-1} g[n]g[n+\frac{lM}{2}]e^{j2\pi\frac{m}{M}n}, \tag{3.18}$$

doi:10.6342/NTU202302942

and the self-interference ρ_{m_0,l_0} can be expressed as

$$\begin{aligned}\rho_{m_0,l_0} &= \sum_{\substack{l=-\infty \\ |l|+|m|\neq 0}}^{\infty} \sum_{m=-m_0}^{M-m_0-1} a_{m+m_0,l+l_0}(-1)^{m_0 l}\Re\left\{\zeta_{m+m_0,l+l_0}\zeta^*_{m_0,l_0}A_{m,l}\right\} \\ &= \sum_{\substack{l=-\infty \\ |l|+|m|\neq 0}}^{\infty} \sum_{m=-m_0}^{M-m_0-1} a_{m+m_0,l+l_0}(-1)^{m_0 l}\Re\left\{j^{(m+l)}A_{m,l}\right\}.\end{aligned} \tag{3.19}$$

From (3.19), we can conclude

1. when $(m+l)$ is odd, we need to suppress the imaginary part of $A_{m,l}$

2. when $(m+l)$ is even and $|l|+|m|\neq 0$, we need to suppress the real part of $A_{m,l}$

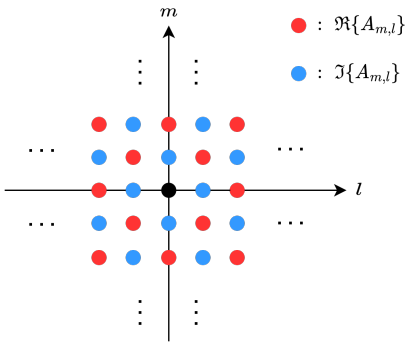

Figure 3.1: Discrete Ambiguity surface

The second property of the prototype filter $g[n]$ can now be formulated as

$$\begin{aligned}&\left|\Im\{A_{m,l}\}\right| < t, \quad \text{for } (m+l) \text{ being odd} \\ &\left|\Re\{A_{m,l}\}\right| < t, \quad \text{for } (m+l) \text{ being even, } |l|+|m|\neq 0,\end{aligned} \tag{Property 2}$$

where t is the threshold of the ambiguity function. The threshold t is highly relative to the signal-to-interference ratio (SIR) of the prototype filter. It should be set as a small number. In addition to the property of NPR, the property of low PSL is also needed to be constructed. We define the union of the set of PSL locations and the set of beginning and

doi:10.6342/NTU202302942

end frequencies in the region of the stopband as

$$\mathbb{W}_s = \left\{ \omega \in \mathbb{R} \middle| \omega \in (\omega_s, \pi),\ \tfrac{d}{d\omega}|G(e^{j\omega})|^2 = 0 \right\} \cup \left\{ \omega_s,\ \pi \right\}, \tag{3.20}$$

where ω_s and $G(e^{j\omega})$ denote stopband frequency point and DTFT of $g[n]$, respectively. Then, the third property or the PSL constraint can be expressed as

$$|G(e^{j\omega})|^2 \leq s, \quad \forall \omega \in \mathbb{W}_s, \tag{Property 3}$$

where s denotes the threshold of PSL. From (Property 1),(Property 2) and (Property 3), we can now intuitively construct the primal optimization problem of FBMC waveform design, it can be expressed as

$$\underset{g[n], s \in \mathbb{R}_+}{\text{minimize}} \quad s \tag{3.21a}$$

$$\text{subject to} \quad |A_{0,0}| = 1 \tag{3.21b}$$

$$\left| \Im\{A_{m,l}\} \right| \leq t, \quad \text{for } (m+l) \text{ being odd} \tag{3.21c}$$

$$\left| \Re\{A_{m,l}\} \right| \leq t, \quad \text{for } (m+l) \text{ being even, } |l| + |m| \neq 0 \tag{3.21d}$$

$$|G(e^{j\omega})|^2 \leq s, \quad \forall \omega \in \mathbb{W}_s. \tag{3.21e}$$

In the next chapter, we will present our proposed approaches to solve this waveform design problem.

doi:10.6342/NTU202302942

Chapter 4 Proposed Approach

doi:10.6342/NTU202302942

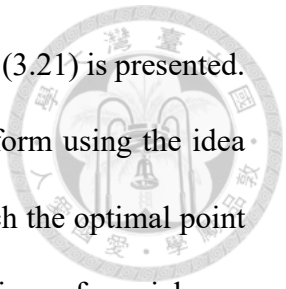

In this chapter, the proposed approach to solve the main problem (3.21) is presented. We first reformulate the primal problem (3.21) to be an equivalent form using the idea of semidefinite relaxation. Then, we propose an algorithm to approach the optimal point of the primal problem. In Section 4.1, we first introduce some definitions of special vectors and matrices to transform the primal problem into several equivalent vector forms. Unfortunately, the equivalent problem is still non-convex so we apply the semidefinite relaxation to it. In Section 4.2, we solve the relaxed problem and use the proposed algorithm to approach the optimal point of the primal problem.

4.1 Reformulated Problem

For simplicity, we transform the original problem (3.21) into vector form. Here, we introduce some definitions of special vectors and matrices. First, we define our target of optimization $g[n]$ to be a vector form that can be expressed as

$$\mathbf{g} = \begin{bmatrix} g_0 & g_1 & \cdots & g_{KM-1} \end{bmatrix}^T \in \mathbb{C}^{KM}, \tag{4.1}$$

where $g_n = g[n]$. Second, we introduce the shift matrix for the demand of derivation, and the upper shift and lower shift matrix are written as

$$\mathbf{U}_{KM} = \begin{bmatrix} 0 & 1 & 0 & \cdots & 0 \\ 0 & 0 & 1 & \cdots & 0 \\ 0 & 0 & 0 & \cdots & 0 \\ \vdots & \vdots & \vdots & \ddots & 1 \\ 0 & 0 & 0 & \cdots & 0 \end{bmatrix}_{KM \times KM} \quad \text{and} \quad \mathbf{D}_{KM} = \begin{bmatrix} 0 & 0 & 0 & \cdots & 0 \\ 1 & 0 & 0 & \cdots & 0 \\ 0 & 1 & 0 & \cdots & 0 \\ \vdots & \vdots & \vdots & \ddots & \vdots \\ 0 & 0 & 0 & 1 & 0 \end{bmatrix}_{KM \times KM}, \tag{4.2}$$

doi:10.6342/NTU202302942

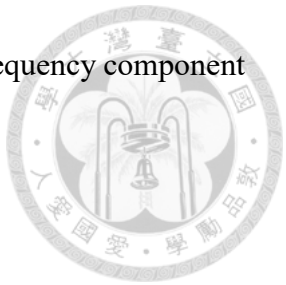

respectively. Third, we introduce diagonal matrix $\mathbf{S}^{'}$ that has only a frequency component on the diagonal. It can be expressed as

$$\mathbf{S}^{'} = \begin{bmatrix} 1 & 0 & 0 & \cdots & 0 \\ 0 & e^{j2\pi\frac{1}{M}} & 0 & \cdots & 0 \\ 0 & 0 & e^{j2\pi\frac{1}{M}\cdot 2} & \cdots & 0 \\ \vdots & \vdots & \vdots & \ddots & 0 \\ 0 & 0 & 0 & \cdots & e^{j2\pi\frac{1}{M}\cdot(KM-1)} \end{bmatrix}_{KM\times KM} \in \mathbb{C}^{KM\times KM}. \tag{4.3}$$

Based on the above definitions, we can rewrite the discrete ambiguity function (3.18) as

$$\begin{aligned} A_{m,l} &= \sum_{n=0}^{KM-1} g[n]g[n+l\cdot\frac{M}{2}]e^{j2\pi\frac{m}{M}n} \\ &= \sum_{n=0}^{KM-1} g[n]e^{j2\pi\frac{m}{M}n}g[n+l\cdot\frac{M}{2}] \\ &= \begin{cases} \mathbf{g}^T(\mathbf{S}^{'})^m(\mathbf{U}_{KM})^{l\cdot\frac{M}{2}}\mathbf{g}, & l\geq 0 \\ \mathbf{g}^T(\mathbf{S}^{'})^m(\mathbf{D}_{KM})^{-l\cdot\frac{M}{2}}\mathbf{g}, & l<0 \end{cases} \\ &= \mathbf{g}^T\mathbf{S}^{(m,l)}\mathbf{g}, \end{aligned} \tag{4.4}$$

where we define $\mathbf{S}^{(m,l)}$ as

$$\mathbf{S}^{(m,l)} = \begin{cases} (\mathbf{S}^{'})^m(\mathbf{U}_{KM})^{l\cdot\frac{M}{2}}, & l\geq 0 \\ (\mathbf{S}^{'})^m(\mathbf{D}_{KM})^{-l\cdot\frac{M}{2}}, & l<0 \end{cases} \in \mathbb{C}^{KM\times KM}. \tag{4.5}$$

The PSL constraint (3.21e) can also be transformed into the vector form as

$$\begin{aligned} |G(e^{j\omega})|^2 &= (\mathbf{g}^T\mathbf{w}^{(\omega)})(\mathbf{g}^T\mathbf{w}^{(\omega)})^H \\ &= \mathbf{g}^T\mathbf{W}^{(\omega)}\mathbf{g}, \end{aligned} \tag{4.6}$$

doi:10.6342/NTU202302942

where

$$\begin{cases} \mathbf{w}^{(\omega)} = \begin{bmatrix} 1 & e^{-j\omega} & e^{-j\omega\cdot 2} & \cdots & e^{-j\omega\cdot(KM-1)} \end{bmatrix}^T \\ \mathbf{W} = \mathbf{w}^{(\omega)}\mathbf{w}^{(\omega)^H} \end{cases}. \tag{4.7}$$

The primal problem can be expressed in an equivalent form as

$$\underset{\mathbf{g}, s\in\mathbb{R}_+}{\text{minimize}} \quad s \tag{4.8a}$$

$$\text{subject to} \quad \mathbf{g}^T\mathbf{g} = 1 \tag{4.8b}$$

$$\left|\mathbf{g}^T\mathbf{S}_I^{(m,l)}\mathbf{g}\right| \le t, \quad \text{for } (m+l) \text{ being odd} \tag{4.8c}$$

$$\left|\mathbf{g}^T\mathbf{S}_R^{(m,l)}\mathbf{g}\right| \le t, \quad \text{for } (m+l) \text{ being even, } |l|+|m| \neq 0 \tag{4.8d}$$

$$\mathbf{g}^T\mathbf{W}^{(\omega)}\mathbf{g} \le s, \quad \forall\omega \in \mathbb{W}_s, \tag{4.8e}$$

where

$$\begin{cases} \mathbf{S}_I^{(m,l)} = \Im\{\mathbf{S}^{(m,l)}\} \in \mathbb{R}^{KM\times KM} \\ \mathbf{S}_R^{(m,l)} = \Re\{\mathbf{S}^{(m,l)}\} \in \mathbb{R}^{KM\times KM}. \end{cases} \tag{4.9}$$

doi:10.6342/NTU202302942

The problem (4.8) is not convex since the constraint function in (4.8b) is not affine. Therefore, we define $\mathbf{G} = \mathbf{g}\mathbf{g}^T \in \mathbb{S}_+^{KM}$, and the problem (4.8) can be reformulated as

$$\underset{\mathbf{G}\in\mathbb{S}_+^{KM}, s\in\mathbb{R}_+}{\text{minimize}} \quad s \tag{4.10a}$$

$$\text{subject to} \quad \text{Tr}(\mathbf{G}) = 1 \tag{4.10b}$$

$$\text{Tr}(\mathbf{G}\mathbf{S}_I^{(m,l)}) \leq t, \quad \text{for } (m+l) \text{ being odd} \tag{4.10c}$$

$$\text{Tr}(\mathbf{G}\mathbf{S}_I^{(m,l)}) \geq -t, \quad \text{for } (m+l) \text{ being odd} \tag{4.10d}$$

$$\text{Tr}(\mathbf{G}\mathbf{S}_R^{(m,l)}) \leq t, \quad \text{for } (m+l) \text{ being even, } |l|+|m| \neq 0 \tag{4.10e}$$

$$\text{Tr}(\mathbf{G}\mathbf{S}_R^{(m,l)}) \geq -t, \quad \text{for } (m+l) \text{ being even, } |l|+|m| \neq 0 \tag{4.10f}$$

$$\text{Tr}(\mathbf{G}\mathbf{W}^{(\omega)}) \leq s, \quad \forall \omega \in \mathbb{W}_s, \tag{4.10g}$$

$$\text{rank}\{\mathbf{G}\} = 1. \tag{4.10h}$$

However, the problem (4.10) is still not convex due to the rank-one constraint (4.10h). Thus, the SDR [19] is applied to relax the rank-one constraint (4.10h). The problem (4.10)

doi:10.6342/NTU202302942

can be rewritten as a convex optimization problem that can be expressed as

$$\underset{\mathbf{G}\in\mathbb{S}_+^{KM},s\in\mathbb{R}_+}{\text{minimize}} \quad s + w \cdot \text{Tr}(\mathbf{G}\mathbf{U}^{(\varphi)}) \tag{4.11a}$$

$$\text{subject to} \quad \text{Tr}(\mathbf{G}) = 1 \tag{4.11b}$$

$$\text{Tr}(\mathbf{G}\mathbf{S}_I^{(m,l)}) \leq t, \quad \text{for } (m+l) \text{ being odd} \tag{4.11c}$$

$$\text{Tr}(\mathbf{G}\mathbf{S}_I^{(m,l)}) \geq -t, \quad \text{for } (m+l) \text{ being odd} \tag{4.11d}$$

$$\text{Tr}(\mathbf{G}\mathbf{S}_R^{(m,l)}) \leq t, \quad \text{for } (m+l) \text{ being even, } |l|+|m| \neq 0 \tag{4.11e}$$

$$\text{Tr}(\mathbf{G}\mathbf{S}_R^{(m,l)}) \geq -t, \quad \text{for } (m+l) \text{ being even, } |l|+|m| \neq 0 \tag{4.11f}$$

$$\text{Tr}(\mathbf{G}\mathbf{W}^{(\omega)}) \leq s, \quad \forall \omega \in \mathbb{W}_s \tag{4.11g}$$

$$\mathbf{G} \succeq 0, \tag{4.11h}$$

where w is a positive penalty weight and $\mathbf{U} \in \mathbb{C}^{KM\times KM}$ is a penalty matrix.

4.2 Proposed Method Based on Dattorro Iterative Algorithm

Even though we relax the equivalent primal problem (4.10) to be relaxed convex problem (4.11), the optimal $\mathbf{G}$ we can obtain from the problem (4.11) is still not the optimal point of the primal problem due to the relaxation we apply. The way to approach the optimal point of the equivalent primal problem (4.10) is to try to make the target variable $\mathbf{G}$ to be rank-one, which fits the constraint (4.10h). Here, we adopt the iterative algorithm proposed by Dattorro [4]. The main idea of this algorithm is to minimize the sum of the smallest eigenvalues, i.e., exploit the equivalence between imposing the constraint $\text{rank}(\mathbf{G}) < r$ (with $\mathbf{G} \in \mathbb{S}_+^n$) and imposing the constraint that the sum of the $n-r$

doi:10.6342/NTU202302942

smallest eigenvalues of $\mathbf{G}$ is equal to zero, which is a straightforward method to solve the problem with rank constraints in engineering. More research on the analytical comparison of algorithms solving the problems with rank constraints can be found in [5].

In the initialization of this algorithm, without loss of generality, we set the penalty matrix $\mathbf{U}^{(0)} = \mathbf{0}_{KM\times KM}$ and $\mathbb{W}_s^{(0)}$ as the set uniformly sampling at the region of stopband with J_s points since we don't know the location of the PSLs in the beginning. Then, we solve the problem (4.11) in every iteration, and $\mathbf{G}^{(\varphi)}$ denote the optimal point obtained from the problem (4.11) in φ-th iteration.

Since the target variable $\mathbf{G}$ is positive semidefinite and symmetric, we can conduct eigendecomposition on $\mathbf{G}^{(\varphi)}$, which can be expressed as

$$\mathbf{G}^{(\varphi)} = \tilde{\mathbf{U}}^{(\varphi)}\tilde{\mathbf{D}}^{(\varphi)}(\tilde{\mathbf{U}}^{(\varphi)})^H, \tag{4.12}$$

where the eigenvalues along the main diagonal of $\tilde{\mathbf{D}}^{(\varphi)}$ is in descending order, i.e., $[\tilde{\mathbf{D}}]_{1,1}^{(\varphi)} \geq [\tilde{\mathbf{D}}]_{2,2}^{(\varphi)} \geq \cdots \geq [\tilde{\mathbf{D}}]_{KM,KM}^{(\varphi)} \geq 0$. Then, the penalty matrix can be designed as

$$\mathbf{U}^{(\varphi)} = [\tilde{\mathbf{U}}^{(\varphi)}]_{\{2,3,\ldots,KM\}} \cdot [\tilde{\mathbf{U}}^{(\varphi)}]_{\{2,3,\ldots,KM\}}^H, \tag{4.13}$$

where $\mathbb{I}$ denote the index set of column vectors of $\tilde{\mathbf{U}}^{(\varphi)}$, and $[\tilde{\mathbf{U}}^{(\varphi)}]_{\{\mathbb{I}\}}$ denote the matrix arranged by $\tilde{\mathbf{U}}^{(\varphi)}$'s column vectors whose indexs are belong to $\mathbb{I}$. With the penalty matrix defined in (4.13), the penalty term $\mathrm{Tr}(\mathbf{G}\mathbf{U}^{(\varphi)})$ in (4.11a) can now be regarded as the sum of all the eigenvalue corresponding to $\mathbf{G}$ without the largest one, i.e., $[\tilde{\mathbf{D}}^{(\varphi)}]_{1,1}$. By adding this penalty term, we can suppress all the eigenvalues except $[\tilde{\mathbf{D}}^{(\varphi)}]_{1,1}$. Then, we set the upper bound ϵ to the ratio $[\tilde{\mathbf{D}}^{(\varphi)}]_{2,2}/[\tilde{\mathbf{D}}^{(\varphi)}]_{1,1}$. This ratio should be set as a strictly small number to ensure the optimal point $\mathbf{G}^*$ approaching rank-one. If the ratio $[\tilde{\mathbf{D}}^{(\varphi)}]_{2,2}/[\tilde{\mathbf{D}}^{(\varphi)}]_{1,1}$ once

doi:10.6342/NTU202302942

meet the upper bound ϵ, the algorithm end.

In addition, during each iteration, the location of the PSLs should be updated. In (φ)-th iteration, the corresponding prototype filter can be expressed as

$$\mathbf{g}^{(\varphi)} = [\tilde{\mathbf{U}}^{(\varphi)}]_{\{1\}} \cdot [\tilde{\mathbf{D}}^{(\varphi)}]_{1,1}. \tag{4.14}$$

Then, we specify the magnitude response $|G^{(\varphi)}(e^{j\omega})|^2$ of $\mathbf{g}^{(\varphi)}$ and find the location of all the PSLs to update $\mathbb{W}_s^{(\varphi)}$. Moreover, the marginal points of the stopband region are also the points we want to suppress, and the updated set $\mathbb{W}_s^{(\varphi+1)}$ in the frequency domain can be expressed as

$$\mathbb{W}_s^{(\varphi+1)} = \left\{ \omega_p \;\middle|\; \omega_p \in (\omega_s, \pi), \left[\frac{d}{d\omega} |G^{(\varphi)}(e^{j\omega})|^2 \right]_{\omega=\omega_p} = 0 \right\} \cup \{\omega_s, \pi\}. \tag{4.15}$$

Since it is difficult to find the zeros of the derivatives of $G^{(\varphi)}(e^{j\omega})$, in practice, we simply find the peaks of $|G^{(\varphi)}(e^{j\omega})|^2$ by calculating the function at a large number, say $N_s = 10000$, of points uniformly and find ω_p's accordingly:

$$\begin{aligned} \mathbb{W}_s^{(\varphi+1)} = \Big\{ \omega_p \;\Big|\; & \omega_p \in (\omega_s, \pi), |G^{(\varphi)}(e^{j\omega_p})|^2 > |G^{(\varphi)}(e^{j\omega_{p+1}})|^2 \text{ and} \\ & |G^{(\varphi)}(e^{j\omega_p})|^2 > |G^{(\varphi)}(e^{j\omega_{p-1}})|^2, p = 0, 1, ..., N_s - 1 \Big\} \cup \{\omega_s, \pi\}. \end{aligned} \tag{4.16}$$

After we make $\mathbf{G}$ to approach rank-one, the target optimal variable $\mathbf{g}$ in (4.8) can now be extract from $\mathbf{G}$, which can be expressed as

$$\mathbf{g} = [\tilde{\mathbf{U}}^{(\varphi-1)}]_{\{1\}} \cdot [\tilde{\mathbf{D}}^{(\varphi-1)}]_{1,1}, \tag{4.17}$$

doi:10.6342/NTU202302942

which is the vector form of the optimal prototype filter.

By the discussion above, the proposed algorithm based on the Dattorro Iterative algorithm [4] is summarized as follows:

Algorithm 1 Proposed Algorithm

Input: w, $\mathbf{S}$;

Output: $\mathbf{g}$;

1: Initialization: $\varphi = 0$, $\mathbf{U}^{(0)} = \mathbf{0}_{KM\times KM}$ and $\mathbb{W}_s^{(0)}$ uniformly sampling at the region of stop-band with J_s points;

2: **repeat**

3: Solve the problem (4.11) to get the optimal solution $\mathbf{G}^{(\varphi)}$.

4: Perform eigendecomposition on $\mathbf{G}^{(\varphi)}$: $\mathbf{G}^{(\varphi)} = \tilde{\mathbf{U}}^{(\varphi)}\tilde{\mathbf{D}}^{(\varphi)}(\tilde{\mathbf{U}}^{(\varphi)})^H$, with the eigenvalues along the main diagonal of $\mathbf{D}^{(\varphi)}$ in descending order, i.e., $[\tilde{\mathbf{D}}^{(\varphi)}]_{1,1} \geq [\tilde{\mathbf{D}}^{(\varphi)}]_{2,2} \geq \cdots \geq [\tilde{\mathbf{D}}^{(\varphi)}]_{KM,KM} \geq 0$.

5: Set $\sigma_1 = [\tilde{\mathbf{D}}^{(\varphi)}]_{1,1}$ and $\sigma_2 = [\tilde{\mathbf{D}}^{(\varphi)}]_{2,2}$.

6: Set the (φ)-th prototype filter as $\mathbf{g}^{(\varphi)} = [\tilde{\mathbf{U}}^{(\varphi)}]_{\{1\}} \cdot \sigma_1$, and update $\mathbb{W}_s$ using (4.16).

7: Update penalty matrix : $\mathbf{U}^{(\varphi+1)} = [\tilde{\mathbf{U}}^{(\varphi)}]_{\{2,3,\cdots,KM\}} \cdot [\tilde{\mathbf{U}}^{(\varphi)}]^H_{\{2,3,\cdots,KM\}}$.

8: If $\left|[(\sigma_2/\sigma_1)^{(\varphi)} - (\sigma_2/\sigma_1)^{(\varphi-1)}]/[(\sigma_2/\sigma_1)^{(\varphi-1)}]\right| < 0.1$, then $w^{(\varphi+1)} = w^{(\varphi)} \cdot 1.01$.

9: $\varphi \leftarrow \varphi + 1$.

10: **until** $\sigma_2/\sigma_1 \leq \epsilon$;

11: Obtain: $\mathbf{g} = [\tilde{\mathbf{U}}^{(\varphi-1)}]_{\{1\}} \cdot \sigma_1$.

Since there are lots of kinds of SDR problems with constraints strict or not, the algorithm 1 doesn't guarantee convergence. From statement 8 in the algorithm 1, we check the ratio (σ_2/σ_1) in every iteration. To avoid the iteration staggering, if the ratio (σ_2/σ_1) doesn't change by ten percent compared with the last iteration, we slightly enhance the penalty weight w by one percent, which makes the iteration converge faster. This trivial way to achieve the convergence of the algorithm 1 is by the method of trial and error.

doi:10.6342/NTU202302942

Chapter 5 Simulation Results

doi:10.6342/NTU202302942

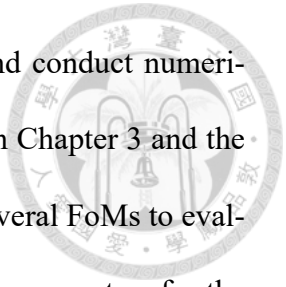

In this chapter, we introduce some figures of merits (FoMs) and conduct numerical simulations to give a comparison between the proposed method in Chapter 3 and the existing prototype filters in [1, 14, 26]. In Section 5.1, we describe several FoMs to evaluate the performance of FBMC filters. In Section 5.2, we specify the parameters for the simulation. In Section 5.3, we compare the different filters with their performance on magnitude response and the FoMs mentioned in Section 5.1. In Section 5.4, we conduct a simulation on bit error rate (BER) in different channels to verify the influence of self-interference caused by the different prototype filters. In Section 5.5, we will show the PSD of the FBMC system by using the different prototype filters, which gives a straightforward perspective to verify the performance on OoBE. The simulation results in this chapter show that the performance of the proposed prototype filter outperforms the filter mentioned previously in maximum side-lobe level (MSL).

5.1 Figure of Merits

In this section, we introduce three FoMs to compare different filters. First, we introduce the signal-to-interference ratio (SIR) which is highly relative to the property of near-perfect reconstruction (NPR) mentioned in Section 2.3.4. Second, we introduce the OoBE which shows the energy leakage out of the passband. Third, we introduce the MSL which caused the maximal interference to the adjacent band.

5.1.1 Signal-to-Interference Ratio (SIR)

For the high quality of reconstruction, SIR is the main factor that affects the performance of the property of NPR at the receiver side. From (3.16) and (3.19), the estimated

doi:10.6342/NTU202302942

staggered PAM symbol can be expressed as

$$\begin{aligned}\hat{a}_{m_0,l_0} &= a_{m_0,l_0} + \underbrace{\sum_{\substack{l=-\infty \\ l\neq 0}}^{\infty} \sum_{\substack{m=-m_0 \\ m\neq 0}}^{M-m_0-1} a_{m+m_0,l+l_0}(-1)^{m_0 l}\Re\left\{j^{(m+l)}A_{m,l}\right\}}_{\text{self-interference}} \\ &= a_{m_0,l_0} + \underbrace{\sum_{\substack{l=-\infty \\ l\neq 0}}^{\infty} \sum_{\substack{m=-m_0 \\ m\neq 0}}^{M-m_0-1} a_{m+m_0,l+l_0}\Re\left\{j^{(m+l)}\langle\, g_{m,l}[n] \mid g_{m_0,l_0}[n]\,\rangle\right\}}_{\text{self-interference}},\end{aligned} \tag{5.1}$$

where $g_{m,l}[n] = g[n - l\cdot\frac{M}{2}]e^{j2\pi\frac{m}{M}(n-l\cdot\frac{M}{2})}$. The simplified representation of the interference power at (m,l)-th point can be represented as

$$\epsilon_{m,l} = \left|\Re\left\{j^{(m+l)}A_{m,l}\right\}\right|^2 = \left|\Re\left\{j^{(m+l)}\langle\, g_{m,l}[n] \mid g_{m_0,l_0}[n]\,\rangle\right\}\right|^2. \tag{5.2}$$

Based on the limited length of filter $g[n]$ and the conjugate symmetry of ambiguity , i.e., $A_{-m,l} = A^*_{m,l}$, we define SIR as

$$\text{SIR} = \frac{1}{\sum_{m=0}^{M-1}\sum_{l=-K+1}^{K-1}\epsilon_{m,l}}. \tag{5.3}$$

5.1.2 Out-of-Band Emission (OoBE)

Moreover, Low OoBE ensures high energy efficiency and low interference to adjacent bands. The In-Band energy, i.e., the energy contained within the frequency range

doi:10.6342/NTU202302942

$|\omega| \leq \omega_s$, can be defined as

$$
\begin{aligned}
E(\omega_s) &= \frac{1}{2\pi}\int_{-\omega_s}^{\omega_s} |G(e^{j\omega})|^2\, d\omega \\
&= \frac{1}{2\pi}\int_{-\omega_s}^{\omega_s} (\sum_{k=0}^{L-1} g[k]e^{-j\omega k})(\sum_{l=0}^{L-1} g[l]e^{-j\omega l})^*\, d\omega \\
&= \frac{1}{2\pi}\int_{-\omega_s}^{\omega_s} (\sum_{k=0}^{L-1}\sum_{l=0}^{L-1} g[k]g[l]e^{-j\omega(k-l)})\, d\omega \\
&= \frac{1}{2\pi}\sum_{k=0}^{L-1}\sum_{l=0}^{L-1} g[k]g[l]\int_{-\omega_s}^{\omega_s} e^{-j\omega(k-l)}\, d\omega \\
&= \sum_{k=0}^{L-1}\sum_{l=0}^{L-1} g[k]g[l]\left\{\tfrac{1}{(k-l)\pi}\cdot\tfrac{e^{j\omega_s(k-l)}-e^{-j\omega_s(k-l)}}{2j}\right\} \\
&= \sum_{k=0}^{L-1}\sum_{l=0}^{L-1} g[k]g[l]\left\{\tfrac{\sin(\omega_s(k-l))}{(k-l)\pi}\right\} \\
&= \sum_{k=0}^{L-1}\sum_{l=0}^{L-1} g[k]g[l]\left\{\tfrac{\sin(\pi\cdot\frac{\omega_s}{\pi}(k-l))}{\pi\cdot\frac{\omega_s}{\pi}(k-l)}\cdot\tfrac{\omega_s}{\pi}\right\} \\
&= \sum_{k=0}^{L-1}\sum_{l=0}^{L-1} g[k]g[l]\left\{\mathrm{sinc}(\tfrac{\omega_s}{\pi}(k-l))\cdot\tfrac{\omega_s}{\pi}\right\} \\
&= \mathbf{g}^T\mathbf{\Gamma}(\omega_s)\mathbf{g},
\end{aligned}
\tag{5.4}
$$

where

$$
\left[\mathbf{\Gamma}(\omega_s)\right]_{k,l} = \frac{\omega_s}{\pi}\mathrm{sinc}\left[(k-l)\tfrac{\omega_s}{\pi}\right], \tag{5.5}
$$

and the OoBE, i.e., the energy outside the frequency range $|\omega| \leq \omega_s$, can be defined as

$$
\bar{E}(\omega_s) = E(\pi) - E(\omega_s) = \mathbf{g}^T[\mathbf{I} - \mathbf{\Gamma}(\omega_s)]\mathbf{g} = \mathbf{g}^T\bar{\mathbf{\Gamma}}(\omega_s)\mathbf{g}, \tag{5.6}
$$

where $\bar{\mathbf{\Gamma}}(\omega_s) = [\mathbf{I} - \mathbf{\Gamma}(\omega_s)]$.

doi:10.6342/NTU202302942

5.1.3 Maximum Sidelobe Level (MSL)

The MSL is the ratio between the maximum side-lobe of $|G(e^{j\omega})|^2$ and the main-lobe level, which can be defined as

$$\text{MSL} = \frac{\max_{\omega \in \mathbb{W}} |G(e^{j\omega})|^2}{|G(e^{j0})|^2}, \tag{5.7}$$

where

$$\mathbb{W} = \left\{ \omega \;\middle|\; \omega \in (0, \pi), \quad \frac{d}{d\omega} |G(e^{j\omega})|^2 = 0 \right\}. \tag{5.8}$$

Notice that the MSL describes the interference generated by $g[n]$ to adjacent bands.

5.2 Simulation Parameters

In this section, we summarize all the parameters used for the simulation. For the design of the proposed prototype filter, by applying Dattorro Iterative Algorithm, we first initialize $\mathbb{W}_s^{(0)}$ by sampling uniformly at the region of stopband with $J_s = 2M + \frac{M}{4}$ points. The overlapping factor is set as $K = 4$ without loss of generality, which is the choice in both [1] and [14], and the number of subcarriers is $M = 32$. The ratio upper bound of the Dattorro Iterative Algorithm is set as $\epsilon = 10^{-9}$ to approach the rank-one matrix $\mathbf{G}$, and the penalty weight is set as $w = 0.01$. When the ratio σ_2/σ_1 doesn't change ten percent between the current iteration and the previous iteration, we increase one percent of the penalty weight for the convergence of the algorithm. Concerning ω_s, it is noteworthy mentioning that such a parameter is set around $\frac{2\pi}{M}$, given the subcarrier bandwidth and separation. In our work, we set $\omega_s = r_s \cdot \frac{2\pi}{M}$, and $r_s = 1,\ 1.1,\ 1.2,\ 1.21,\ 1.3$. To suppress the SIR caused by the filters, we set $t = 2 \cdot 10^{-4}$.

doi:10.6342/NTU202302942

For the BER performance, the subcarrier spacing F_o is set as 15 kHz corresponding with the symbol interval $T_o = 1/F_o$ and the sample interval $T_s = T_o/M$. The modulation scheme is uncoded 16-QAM followed by OQAM processing. To verify the BER performance, we considered different types of channel models. For the flat fading channel, we choose the AWGN channel and Flat Rayleigh fading channel. For the frequency selective channel, we use the power delay profiles from ITU-R (International Telecommunication Recommendation Radiocommunication Sector) [22], and we will verify the performance on ITU-R-Pedestrian-A (ITU-R-PA) and ITU-R-Vehicular-A (ITU-R-VA) multipath channel. The number of equalizer taps is set as $L_w = 4$. In each BER curve, we conduct 20000 Monte Carlo trials with 100 QAM symbol frames per trial in the SNR range set as $[0, 30]$ dB.

5.3 Magnitude Response & FoMs

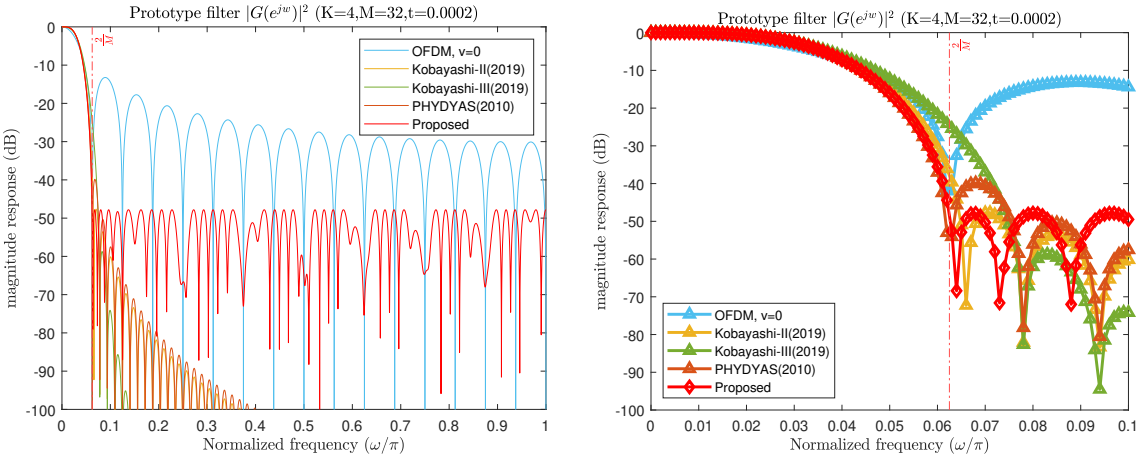

Figure 5.1: Magnitude response $|G(e^{j\omega})|^2$, $r_s = 1$

Throughout Figures 5.1 - 5.4, we can observe that the MSL becomes lower when we slightly increase the value of r_s, i.e., increase the stopband frequency ω_s. But if we increase the stopband frequency too much, the undesired high MSL will occur, such as in

doi:10.6342/NTU202302942

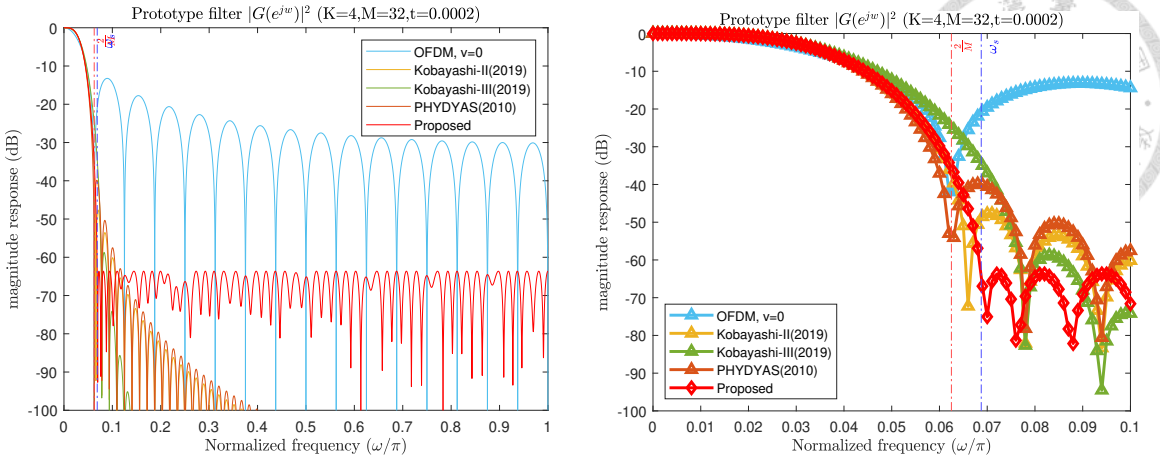

Figure 5.2: Magnitude response $|G(e^{j\omega})|^2$, $r_s = 1.1$

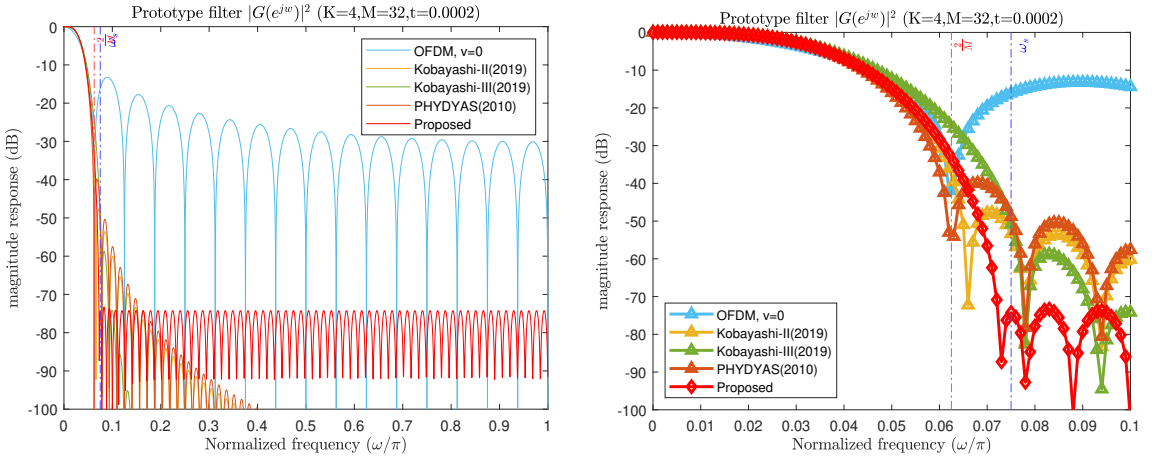

Figure 5.3: Magnitude response $|G(e^{j\omega})|^2$, $r_s = 1.2$

Figure 5.5. Note that under practical regulations such as spectrum emission mask (SEM) or adjacent channel leakage ratio (ACLR), both CP-less OFDM and CP-OFDM require huge amounts of guardband due to the slow decay of their frequency responses. This is also a cause of decreasing spectral efficiency [13]. Out-of-Band emission of multicarrier modulation techniques depends on the power spectral distribution of filters. The main requirement to choose a better filter is choosing a filter with a smaller side-lobe [6].

The comparison between the proposed prototype filter and the filters mentioned in Chapter 3 is summarized in Table 5.1. In the aspect of MSL, the performance of the proposed prototype filter ($r_s = 1.21$) is the best, and it outperforms the previous works

doi:10.6342/NTU202302942

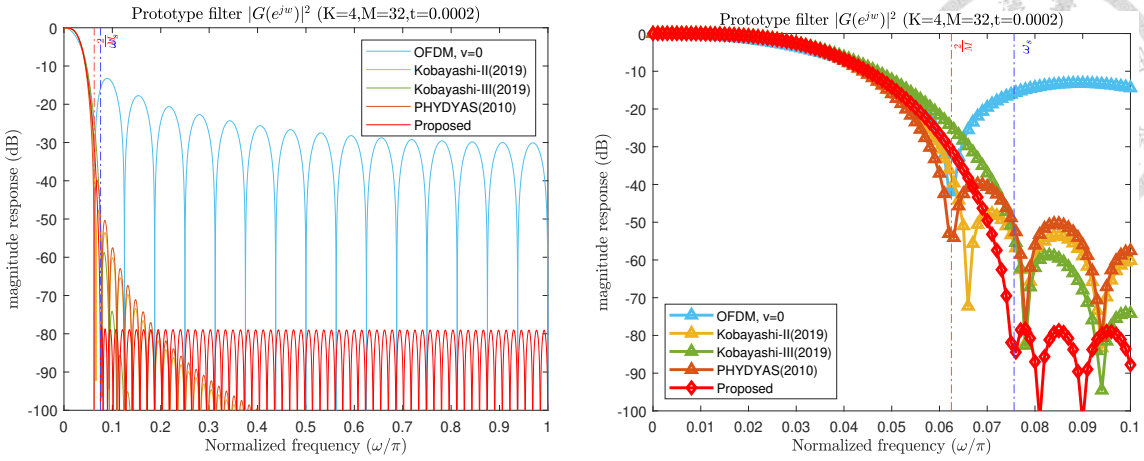

Figure 5.4: Magnitude response $|G(e^{j\omega})|^2$, $r_s = 1.21$

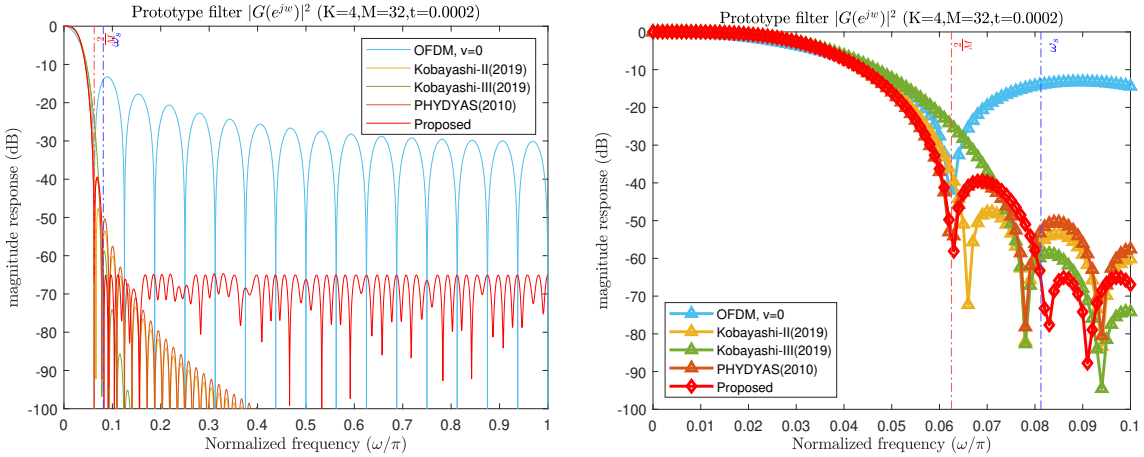

Figure 5.5: Magnitude response $|G(e^{j\omega})|^2$, $r_s = 1.3$

for 20 dB, i.e., the proposed filter has the least interference to the adjacent band, which is achieved by sacrificing a little loss of bandwidth (BW). The loss of bandwidth concerning the strictly frequency stopband point $\omega_s = \frac{2\pi}{M}$ can be expressed as

$$\frac{\text{BW}\ (\omega_s = \frac{2\pi}{M} \cdot r_s)}{\text{BW}\ (\omega_s = \frac{2\pi}{M})} - 1 = \left(\frac{(M + 2r_s - 1)\omega_s}{(M+1)\omega_s} \bigg|_{\omega_s = \frac{2\pi}{M}} - 1 \right) \times 100\%. \tag{5.9}$$

For instance, when $M = 32$ and $r_s = 1.21$, based on (5.9), the loss of bandwidth of the proposed filter is 1.27%. From the perspective of the OoBE, the Kobayashi-II(2019)[14] has the best performance, which is attributed to the property of the spectrum decay that we don't concern about. Since spectrum decay is not an important property, we only need

doi:10.6342/NTU202302942

Prototype Filter	SIR[dB]	MSL[dB]	$\bar{E}(\frac{2\pi}{M})$[dB]
PHYDYAS(2010)	65.20	-39.85	-45.61
OFDP(1996)	59.86	-38.33	-35.45
Kobayashi-II(2019)	68.09	-47.66	-50.09
Kobayashi-III(2019)	51.27	-58.73	-35.20
Proposed ($r_s = 1$)	41.60	-47.82	-36.69
Proposed ($r_s = 1.1$)	50.98	-63.64	-47.00
Proposed ($r_s = 1.2$)	58.64	-74.23	-45.56
Proposed ($r_s = 1.21$)	59.80	-78.02	-42.79
Proposed ($r_s = 1.3$)	52.38	-39.45	-44.52

Table 5.1: Prototype Filter Comparison

to ensure that all the PSL is as low as possible. For the discussion of the influence of different SIR, we will take a look at the performance in BER curves.

5.4 BER Performance

In this section, we perform the simulation to evaluate the BER performances of the proposed FBMC waveform against previously reported waveforms in different channel models. We choose the proposed prototype filter ($r_s = 1.21$) which has the best performance in several FoMs to compare with filters mentioned previously. The numerical results can be observed in the following figures:

Figures 5.6, 5.7, 5.8, and 5.9 show the BER curves for different filters in AWGN, Rayleigh channel, ITU-R-PA [22], and ITU-R-VA channels [22], respectively. By observation, we can see that the BER curves for all the filters are exactly the same. The reason for this phenomenon is caused by the high SIR for the filters, which can be checked in Table 5.1. When BER curves are located at the SNR range from 0 dB to 30 dB, the noise and the channel effect are the factors dominating the performance since the SIR of all the filters are higher than 40 dB. This result also indicates the property of NPR given by the well-designed filter is constructed perfectly.

doi:10.6342/NTU202302942

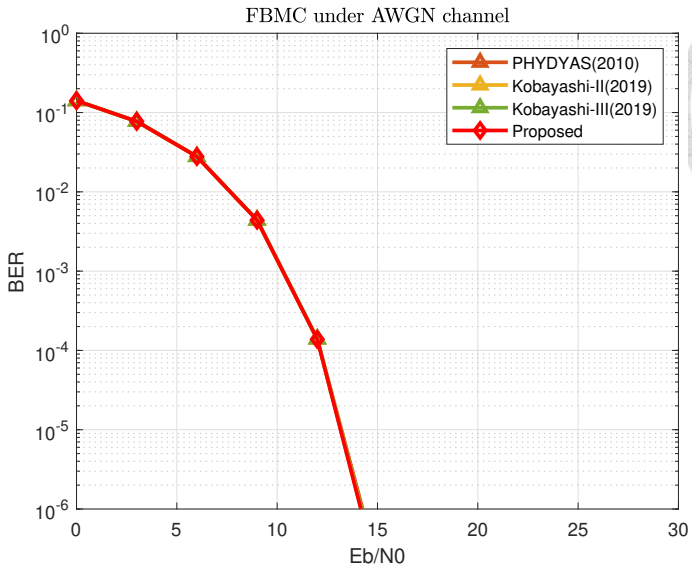

Figure 5.6: BER performance in AWGN channel

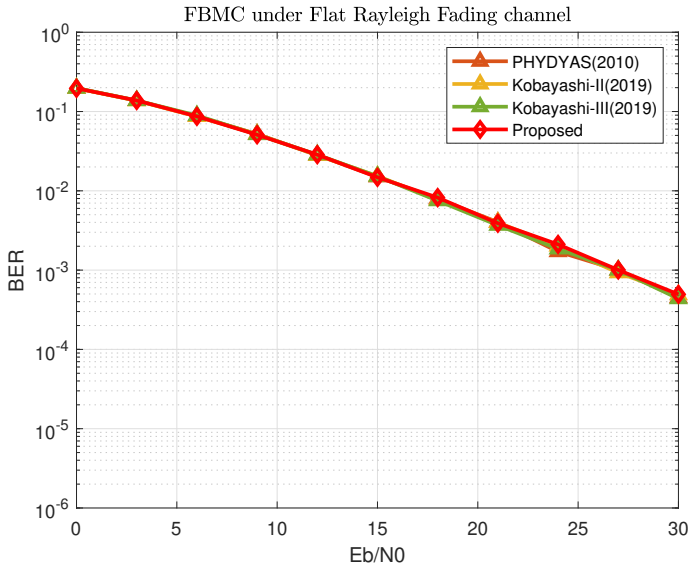

Figure 5.7: BER performance in Rayleigh flat fading channel

5.5 Power Spectral Density (PSD)

In this section, we give a comparison between the filters on the performance of power spectral density (PSD), which is a more straightforward way to specify the performance of out-of-band emission (OoBE) mentioned in Section 5.1.2. Here, we introduce the derivation of the equation of PSD for the FBMC system. We first recall the transmitted signal

doi:10.6342/NTU202302942

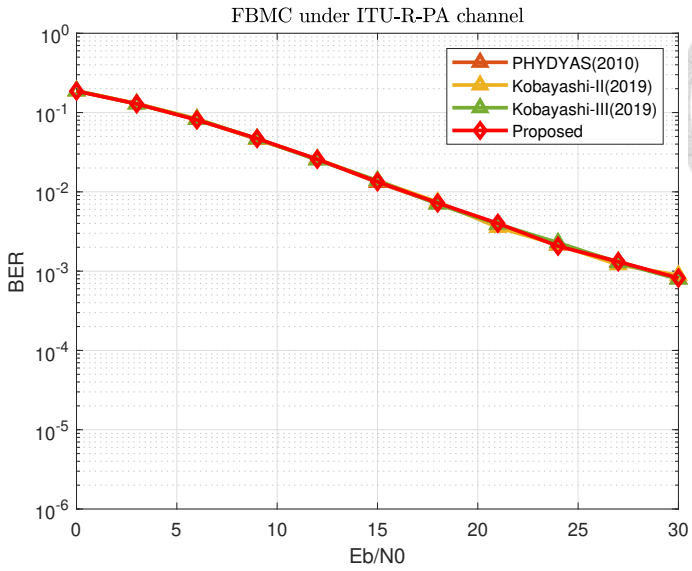

Figure 5.8: BER performance in ITU-R-PA channel

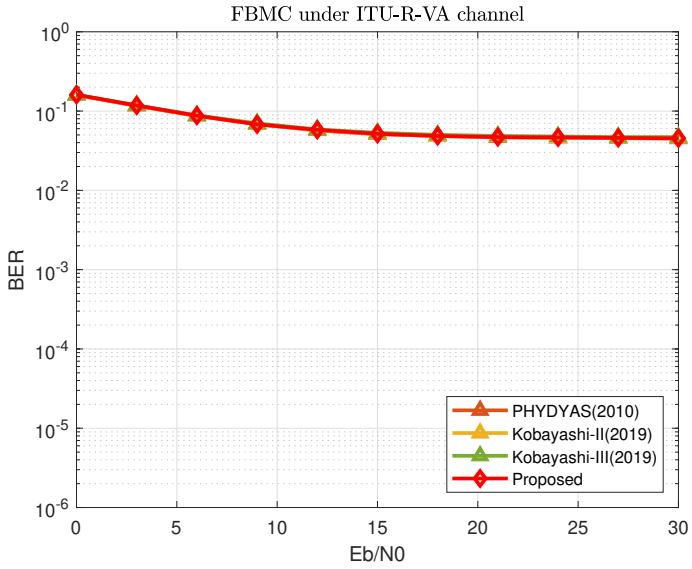

Figure 5.9: BER performance in ITU-R-VA channel

mentioned in (2.5):

$$x[n] = \sum_{m\in\mathcal{M}} \sum_{l=-\infty}^{\infty} a_{m,l}\zeta_{m,l} g[n - l \cdot \frac{M}{2}] e^{j2\pi \frac{m}{M}(n - l\cdot\frac{M}{2})}, \tag{5.10}$$

where $\mathcal{M}$ denotes the used subcarrier index set. Then, we will show that the discrete time random process $x[n]$ is a cyclo wide sense stationary (CWSS) with period M if it satisfies

doi:10.6342/NTU202302942

the following two conditions [15]:

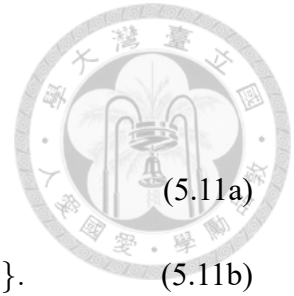

$$E\{x[n+M]\} = E\{x[n]\} \tag{5.11a}$$

$$E\{x[n]x^*[n-n']\} = E\{x[n+M]x^*[n+M-n']\}. \tag{5.11b}$$

We can justify the transmitted signal $x[n]$ satisfying the first condition (5.11a) by the following equation

$$\begin{aligned}
&E\{x[n+M]\} \\
=&E\{\sum_{m\in\mathcal{M}}\sum_{l=-\infty}^{\infty} a_{m,l}\zeta_{m,l}g[n+M-l\cdot\frac{M}{2}]e^{j2\pi\frac{m}{M}(n-l\cdot\frac{M}{2})}\} \\
=&\sum_{m\in\mathcal{M}}\sum_{l=-\infty}^{\infty} E\{a_{m,l}\}\zeta_{m,l}g[n+M-l\cdot\frac{M}{2}]e^{j2\pi\frac{m}{M}(n-l\cdot\frac{M}{2})} \\
=&\sum_{m\in\mathcal{M}}\sum_{l=-\infty}^{\infty} E\{a_{m,l}\}\zeta_{m,l}g[n-l\cdot\frac{M}{2}]e^{j2\pi\frac{m}{M}(n-l\cdot\frac{M}{2})} \\
=&E\{x[n]\}.
\end{aligned} \tag{5.12}$$

For the second condition (5.11b), we first expand the LHS of this condition:

$$\begin{aligned}
&E\{x[n]x^*[n-n']\} \\
=&E\{(\sum_{m\in\mathcal{M}}\sum_{l=-\infty}^{\infty} a_{m,l}\zeta_{m,l}g[n-l\cdot\frac{M}{2}]e^{j2\pi\frac{m}{M}(n-l\cdot\frac{M}{2})}) \\
&\cdot(\sum_{m'\in\mathcal{M}}\sum_{l'=-\infty}^{\infty} a^*_{m',l'}\zeta^*_{m',l'}g[n-l'\cdot\frac{M}{2}]e^{j2\pi\frac{m'}{M}(n-l'\cdot\frac{M}{2})})\} \\
=&\sum_{m\in\mathcal{M}}\sum_{m'\in\mathcal{M}}\sum_{l=-\infty}^{\infty}\sum_{l'=-\infty}^{\infty} E\{a_{m,l}a^*_{m',l'}\}\zeta_{m,l}\zeta^*_{m',l'}g[n-l\cdot\frac{M}{2}]g[n-n'-l'\cdot\frac{M}{2}] \\
&\cdot e^{j2\pi\frac{m}{M}(n-l\cdot\frac{M}{2})}e^{-j2\pi\frac{m'}{M}(n-n'-l'\cdot\frac{M}{2})}.
\end{aligned} \tag{5.13}$$

doi:10.6342/NTU202302942

Since $a_{m,l}$ is statistically independent corresponding to index m and l, we have

$$E\{a_{m,l}a^*_{m',l'}\} = \begin{cases} \sigma_a^2, & \text{when } m = m', l = l' \\ 0, & \text{otherwise} \end{cases}, \tag{5.14}$$

where σ^2 denote the average symbol power of $a_{m,l}$. Then (5.13) can be reformulated as

$$\begin{aligned} &E\{x[n]x^*[n-n']\} \\ =&\sigma_a^2 \sum_{m\in\mathcal{M}} \sum_{l=-\infty}^{\infty} g[n-l\cdot\frac{M}{2}]g[n-n'-l\cdot\frac{M}{2}]e^{j2\pi\frac{m}{M}n'} \end{aligned} \tag{5.15}$$

Similarly, the RHS of condition (5.11b) can be written as

$$\begin{aligned} &E\{x[n+M]x^*[n+M-n']\} \\ =&\sigma_a^2 \sum_{m\in\mathcal{M}} \sum_{l=-\infty}^{\infty} g[n+M-l\cdot\frac{M}{2}]g[n+M-n'-l\cdot\frac{M}{2}]e^{j2\pi\frac{m}{M}n'}. \end{aligned} \tag{5.16}$$

Since $g[n-l\cdot\frac{M}{2}]g[n-n'-l\cdot\frac{M}{2}]$ is a periodic signal with period M, we can conclude the condition (5.11b) is satisfied. Therefore, $x[n]$ is the CWSS process. By satisfying these conditions [15], the average autocorrelation function of $x[n]$ can now be written as

$$\begin{aligned} R_x[n'] &= \frac{1}{M}\sum_{n=0}^{M-1} E\{x[n]x^*[n-n']\} \\ &= \frac{\sigma_a^2}{M}\sum_{n=0}^{M-1}\sum_{m\in\mathcal{M}}\sum_{l=-\infty}^{\infty} g[n-l\cdot\frac{M}{2}]g[n-n'-l\cdot\frac{M}{2}]e^{j2\pi\frac{m}{M}n'} \end{aligned} \tag{5.17}$$

doi:10.6342/NTU202302942

Based on the definition (5.17), the average power spectral density (PSD) is DTFT of $R_x[n']$

$$
\begin{aligned}
S_x(e^{j2\pi f}) &= \sum_{n'=-\infty}^{\infty} R_x[n'] e^{-j2\pi f n'} \\
&= \frac{\sigma_a^2}{M} \sum_{n'=-\infty}^{\infty} \sum_{n=0}^{M-1} \sum_{m\in\mathcal{M}} \sum_{l=-\infty}^{\infty} g[n - l\cdot\frac{M}{2}] g[n - n' - l\cdot\frac{M}{2}] e^{-j2\pi(f-\frac{m}{M})n'} \\
&= \frac{\sigma_a^2}{M} \sum_{m\in\mathcal{M}} \sum_{l=-\infty}^{\infty} \sum_{n=0}^{M-1} g[n - l\cdot\frac{M}{2}] e^{-j2\pi(f-\frac{m}{M})(n-l\cdot\frac{M}{2})} \\
&\quad \cdot \Big(\sum_{n'=-\infty}^{\infty} g[n - n' - l\cdot\frac{M}{2}] e^{-j2\pi(f-\frac{m}{M})(n-n'-l\cdot\frac{M}{2})} \Big)^* \\
&= \frac{\sigma_a^2}{M} \sum_{m\in\mathcal{M}} |G_0(e^{j2\pi(f-\frac{m}{M})})|^2,
\end{aligned}
\tag{5.18}
$$

where $G_0(e^{j2\pi f}) = \sum_{n=0}^{KM-1} g[n] e^{-j2\pi f n}$. Based on the (5.18), we can now show the PSD of the proposed filter. We choose the proposed filter ($r_s = 1.21$) which has the best performance on MSL to compare with other filters. The number of total usable subcarriers is $M = 32$. We conduct the PSD with the used subcarrier set $\mathcal{M} = \{-3, -2, -1, 0, 1, 2, 3\}$. The numerical result is shown as Figure 5.10. We can see that the PSD of the FBMC system using the proposed filter has the lowest MSL, i.e., the least interference to the adjacent band.

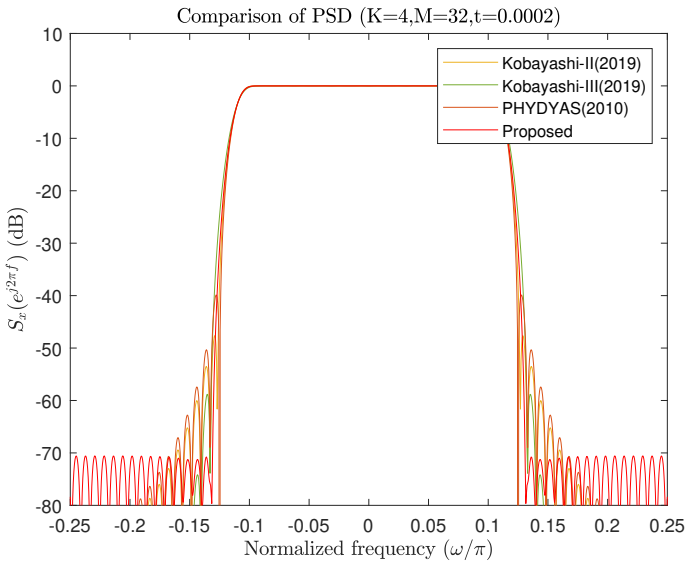

Figure 5.10: Comparison of PSD

doi:10.6342/NTU202302942

Chapter 6 Conclusion & Future Work

doi:10.6342/NTU202302942

6.1 Conclusion

Throughout this thesis, we propose a novel optimization problem to design the prototype filter for the FBMC-OQAM system and solve it by the proposed algorithm. In the proposed optimization problem, we emphasize suppressing all the PSLs, which wasn't a concern in the past work. Based on this concern, the MSL of the proposed prototype filter is much lower than the previous works, which causes the least interference to the adjacent band. In the simulation results of BER, the proposed filter has the same performance as the others since the property of NPR is achieved by the high SIR. Though the proposed filter outperforms the other filters, it must sacrifice approximately one percent of bandwidth, i.e., a little loss of spectral efficiency.

6.2 Future Work

In the past decades, there were still lots of research on prototype filter design [23]. Those filters were also designed for low OoBE or low PSL even though they were not designed for FBMC. Maybe, we can apply these filters to the FBMC system to achieve low OoBE and NPR as well.

Due to the long filters FBMC adopts, the system latency of FBMC is greater than OFDM. Therefore, the short prototype filters are preferred for communication scenarios in the future. To reduce the system latency, there was some research on short prototype filters [16], [20], [18] which are worth checking out. Moreover, there is more novel research on FBMC systems such as satellite communication [3]. In addition to the filter/waveform design of the FBMC system, a new structure for the FBMC system is another topic worth

doi:10.6342/NTU202302942

researching.

doi:10.6342/NTU202302942

References

[1] M. Bellanger, D. Le Ruyet, D. Roviras, M. Terré, J. Nossek, L. Baltar, Q. Bai, D. Waldhauser, M. Renfors, T. Ihalainen, et al. Fbmc physical layer: a primer. PHYDYAS, January, 25(4):7–10, 2010.

[2] M. G. Bellanger. Specification and design of a prototype filter for filter bank based multicarrier transmission. In 2001 IEEE International Conference on Acoustics, Speech, and Signal Processing. Proceedings (Cat. No. 01CH37221), volume 4, pages 2417–2420. IEEE, 2001.

[3] M. Caus, A. I. Pérez-Neira, J. Bas, and L. Blanco. New satellite random access preamble design based on pruned dft-spread fbmc. IEEE Transactions on Communications, 68(7):4592–4604, 2020.

[4] J. Dattorro. Convex optimization & Euclidean distance geometry. Lulu. com, 2010.

[5] R. A. Delgado, J. C. Agüero, and G. C. Goodwin. A rank-constrained optimization approach: Application to factor analysis. IFAC Proceedings Volumes, 47(3):10373–10378, 2014.

[6] H. T. Dumari, D. J. Gelmecha, R. K. Shakya, R. S. Singh, et al. Ber and psd improvement of fbmc with higher order qam using hermite filter for 5g wireless communication and beyond. Journal of Electrical and Computer Engineering, 2023, 2023.

doi:10.6342/NTU202302942

[7] B. Farhang-Boroujeny. Ofdm versus filter bank multicarrier. IEEE signal processing magazine, 28(3):92–112, 2011.

[8] B. Farhang-Boroujeny and R. Kempter. Multicarrier communication techniques for spectrum sensing and communication in cognitive radios. IEEE Communications Magazine, 46(4):80–85, 2008.

[9] B. Farhang-Boroujeny and C. Yuen. Cosine modulated and offset qam filter bank multicarrier techniques: a continuous-time prospect. EURASIP Journal on Advances in Signal Processing, 2010:1–16, 2010.

[10] T. Ihalainen, T. Hidalgo Stitz, M. Rinne, and M. Renfors. Channel equalization in filter bank based multicarrier modulation for wireless communications. EURASIP Journal on Advances in Signal Processing, 2007:1–18, 2006.

[11] T. Ihalainen, A. Ikhlef, J. Louveaux, and M. Renfors. Channel equalization for multi-antenna fbmc/oqam receivers. IEEE transactions on vehicular technology, 60(5):2070–2085, 2011.

[12] T. Ihalainen, T. H. Stitz, and M. Renfors. Efficient per-carrier channel equalizer for filter bank based multicarrier systems. In 2005 IEEE International Symposium on Circuits and Systems, pages 3175–3178. IEEE, 2005.

[13] C. Kim, Y. H. Yun, K. Kim, and J.-Y. Seol. Introduction to qam-fbmc: From waveform optimization to system design. IEEE Communications Magazine, 54(11):66–73, 2016.

[14] R. T. Kobayashi and T. Abrão. Fbmc prototype filter design via convex optimization. IEEE Transactions on Vehicular Technology, 68(1):393–404, 2019.

doi:10.6342/NTU202302942

[15] Y.-P. Lin, S.-M. Phoong, and P. Vaidyanathan. Filter bank transceivers for OFDM and DMT systems. Cambridge University Press, 2010.

[16] H. S. Malvar. Modulated qmf filter banks with perfect reconstruction. Electronics letters, 26(13):906–907, 1990.

[17] S. Mirabbasi and K. Martin. Overlapped complex-modulated transmultiplexer filters with simplified design and superior stopbands. IEEE Transactions on Circuits and Systems II: Analog and Digital Signal Processing, 50(8):456–469, 2003.

[18] J. Nadal, C. A. Nour, and A. Baghdadi. Design and evaluation of a novel short prototype filter for fbmc/oqam modulation. IEEE access, 6:19610–19625, 2018.

[19] Y. Nesterov. Semidefinite relaxation and nonconvex quadratic optimization. Optimization methods and software, 9(1-3):141–160, 1998.

[20] D. Pinchon, P. Siohan, and C. Siclet. Design techniques for orthogonal modulated filterbanks based on a compact representation. IEEE Transactions on signal processing, 52(6):1682–1692, 2004.

[21] A. J. Ramadhan. Implementation of 5g fbmc phydyas prototype filter. International Journal of Applied Engineering Research, 12(23):13476–13481, 2017.

[22] I.-R. Recommendation. Guidelines for evaluation of radio transmission technologies for imt-2000. Rec. ITU-R M. 1225, 1997.

[23] A. Sahin, I. Guvenc, and H. Arslan. A survey on multicarrier communications: Prototype filters, lattice structures, and implementation aspects. IEEE communications surveys & tutorials, 16(3):1312–1338, 2013.

doi:10.6342/NTU202302942

[24] D. Slepian. Prolate spheroidal wave functions, fourier analysis, and uncertainty—v: The discrete case. Bell System Technical Journal, 57(5):1371–1430, 1978.

[25] A. Vahlin and N. Holte. Optimal finite duration pulses for ofdm. In 1994 IEEE GLOBECOM. Communications: The Global Bridge, pages 258–262. IEEE, 1994.

[26] A. Vahlin and N. Holte. Optimal finite duration pulses for ofdm. IEEE Transactions on communications, 44(1):10–14, 1996.

[27] R. Zakaria and D. Le Ruyet. A novel filter-bank multicarrier scheme to mitigate the intrinsic interference: Application to mimo systems. IEEE Transactions on Wireless Communications, 11(3):1112–1123, 2012.

doi:10.6342/NTU202302942